

Comprehensive Assessment of the Too-Big-to-Fail Problem

Fangzhou Jiang^{*} & Frank C. van den Bosch

Department of Astronomy, Yale University, New Haven, CT 06511, USA

ABSTRACT

We use a semi-analytical model for the substructure of dark matter haloes to assess the too-big-to-fail (TBTf) problem. The model accurately reproduces the average subhalo mass and velocity functions, as well as their halo-to-halo variance, in N -body simulations. We construct thousands of realizations of Milky Way (MW) size host haloes, allowing us to investigate the TBTf problem with unprecedented statistical power. We examine the dependence on host halo mass and cosmology, and explicitly demonstrate that a reliable assessment of TBTf requires large samples of hundreds of host haloes. We argue that previous statistics used to address TBTf suffer from the look-elsewhere effect and/or disregard certain aspects of the data on the MW satellite population. We devise a new statistic that is not hampered by these shortcomings, and, using only data on the 9 known MW satellite galaxies with $V_{\max} > 15 \text{ km s}^{-1}$, demonstrate that $1.4^{+3.3}_{-1.1}\%$ of MW-size host haloes have a subhalo population in statistical agreement with that of the MW. However, when using data on the MW satellite galaxies down to $V_{\max} = 8 \text{ km s}^{-1}$, this MW consistent fraction plummets to $< 5 \times 10^{-4}$ (at 68% CL). Hence, if it turns out that the inventory of MW satellite galaxies is complete down to 8 km s^{-1} , then the maximum circular velocities of MW satellites are utterly inconsistent with Λ CDM predictions, unless baryonic effects can drastically increase the spread in V_{\max} values of satellite galaxies compared to that of their subhaloes.

Key words: methods: analytical — methods: statistical — galaxies: haloes — cosmology: dark matter — Galaxy: halo

1 INTRODUCTION

The Λ +cold dark matter (Λ CDM) paradigm of structure formation has been remarkably successful in explaining cosmic structure covering a wide range in redshift and scale. However, on small scales, at low redshifts, a number of potential problems have been identified regarding the abundance and/or structural properties of dark matter (sub)haloes and their associated (satellite) galaxies. In the order in which they have been introduced, these are the ‘cusp-core’ problem, according to which the cuspy central density profiles of CDM haloes predicted by dark-matter-only simulations are inconsistent with observed rotation curves (e.g., Flores & Primack 1994; Moore 1994; Kuzio de Naray, McGaugh & de Blok 2008; Trachternach et al. 2008; de Blok 2010; Oh et al. 2011; but see also van den Bosch & Swaters 2001 and Dutton et al. 2005), the ‘missing-satellite’ problem, highlighting the large discrepancy between the predicted number of CDM subhaloes per host halo and the much smaller number of satellite galaxies detected around host galaxies such as the Milky Way and M31 (e.g., Klypin et al. 1999; Moore et al. 1999), and the ‘too big to fail’

(TBTf) problem, which basically refers to the overabundance of *massive, dense* subhaloes predicted by CDM compared to the observed number of relatively *luminous* satellite galaxies of the Milky Way or the Local Group (e.g., Boylan-Kolchin, Bullock & Kaplinghat 2011, 2012; Martinez 2013; Garrison-Kimmel et al. 2014a, Tollerud, Boylan-Kolchin & Bullock 2014).

In this paper we focus on the TBTf problem (hereafter simply ‘TBTf’), which is generally considered the most difficult to reconcile with Λ CDM, and which has spurred a frenzy of papers offering possible solutions and/or advocating modifications of the standard paradigm. This includes suggestions to change the nature of the dark matter from ‘cold’ to either ‘warm’ or ‘self-interacting’ (e.g., Macció & Fontanot 2010; Vogelsberger, Zavala & Loeb 2012; Lovell et al. 2012; Anderhalden et al. 2013; Rocha et al. 2013; Shao et al. 2013; Polisensky & Ricotti 2014), relatively small changes in the normalization, σ_8 , and/or spectral index, n_s , of the initial power spectrum (e.g., Polisensky & Ricotti 2014), a highly stochastic star formation efficiency for galactic subhaloes, so that a fraction of the more massive subhaloes remain dark (e.g., Kuhlen, Madau & Krumholz 2013; Rodriguez-Puebla, Avila-Reese & Drory 2013a,b), lowering the mass of the MW host halo to $\sim 10^{11.8} h^{-1} M_{\odot}$ (Di Cintio et al. 2011; Wang et

^{*} E-mail:fangzhou.jiang@yale.edu

al. 2012; Vera-Ciro et al. 2013), and enhanced tidal (impulsive) heating of satellite galaxies due to the stellar disk of the Milky Way (Zolotov et al. 2012; Brooks & Zolotov 2014; Arraki et al. 2014).

Despite all this interest in TBTF, we still lack consensus regarding both its formulation and its severity. In fact, the TBTF problem has been formulated in a few subtly different ways. For example, Wang et al. (2012) express it as a problem of missing massive satellites; high-resolution N -body simulations of Milky-Way (MW) size host haloes reveal of the order of 10 subhaloes per host with a maximum circular velocity $V_{\max} \gtrsim 25 \text{ km s}^{-1}$ (e.g., Strigari et al. 2007; Madau, Diemand & Kuhlen 2008; Boylan-Kolchin et al. 2011). Yet, only two MW satellite galaxies (the large and small Magellanic clouds, hereafter LMC and SMC) are believed to have associated subhaloes that meet this criterion. We shall refer to this as the ‘massive subhaloes formulation’ of TBTF. A related expression of TBTF is that the MW reveals a gap in the V_{\max} -distribution of its satellite galaxies. There are no satellite galaxies known with $25 \text{ km s}^{-1} \lesssim V_{\max} \lesssim 55 \text{ km s}^{-1}$, something that is not reproduced in numerical simulations (e.g., Boylan-Kolchin et al. 2012, Cautun et al. 2014b). We shall refer to this as the ‘gap formulation’ of TBTF. Finally, in what we call the ‘density formulation’ of TBTF, it is argued that the (central) *densities* of dark matter subhaloes are too high compared to the central densities in satellite galaxies as inferred from their kinematics (e.g., Boylan-Kolchin et al. 2011; Purcell & Zentner 2012). In this paper we will compare all three formulations, and point out how and where they differ. In particular, we will point out how some of the solutions listed above may solve TBTF in one formulation, but not in the other(s).

As to the severity of TBTF, the lack of consensus largely owes to poor statistics. On the observational side, since TBTF relates to low-luminosity satellite galaxies, which can only be observed in the local neighborhood, the observational ‘evidence’ for a TBTF problem is limited to the MW and M31. Ideally, one would like to test how common this problem is in other host haloes, spanning a range in halo masses and environments. On the theoretical side, the TBTF problem was originally identified using a sample of only 6 simulated MW-size host haloes from the Aquarius project (Springel et al. 2008). More recently, the sample size of high resolution MW-size haloes has grown to the order of 100, with the ELVIS (Garrison-Kimmel et al. 2014a) and c125-2048 (Mao, Williamson & Wechsler 2015) suites each adding of order 50. However, as we demonstrate in this paper, accurately capturing the halo-to-halo variance, and characterizing the severity of TBTF at percent level accuracy, requires of order a thousand realizations of MW-size host haloes with subhaloes resolved down to $V_{\max} \sim 10 \text{ km s}^{-1}$. This is immensely challenging, even for the largest supercomputers available to date (see discussion in van den Bosch et al. 2014).

Because of these statistical drawbacks, some authors have resorted to semi-analytical models (Purcell & Zentner 2012) or empirical extrapolations of large simulations (Cautun et al. 2014a,b) to generate large samples of well-resolved MW-size haloes. In particular, Purcell & Zentner (2012; PZ12 hereafter) use a model developed by Zentner et al. (2005) to generate thousands of MW-size haloes, and claim that at least $\sim 10\%$ of MW-size haloes are free from the TBTF prob-

lem (using the density formulation). However, this study suffers from three drawbacks. First of all, the halo merger trees they use, and which are the backbone of their analytical model, are constructed using the method of Somerville & Kolatt (1999), which has been shown to be significantly and systematically biased (Zhang, Fakhouri & Ma 2008; Jiang & van den Bosch 2014a). Second, their recipe for computing V_{\max} of subhaloes is oversimplified, resulting in unrealistic density estimates. And finally, they only address TBTF in the density formulation, and it therefore remains to be seen what their model predicts regarding the other two formulations.

In this study, we revisit the TBTF problem using a semi-analytical model that we developed and tested in Jiang & van den Bosch (2014b; hereafter Paper I) and van den Bosch & Jiang (2014; hereafter Paper II). The model uses accurate halo merger trees, and well-calibrated (yet simple) recipes for the tidal stripping and disruption of subhaloes. We demonstrate that the model accurately reproduces the halo-to-halo variance of subhalo properties found in numerical simulations, and use it to gauge the severity of TBTF in all three formulations discussed above. We examine the dependence on host halo mass and cosmology, and explicitly demonstrate that numerical simulation suites with of order 50 host haloes can only assess TBTF statistics at ~ 10 percent accuracy. Finally, we show that all three formulations of TBTF either are hampered by the ‘look-elsewhere effect’ or disregard certain aspects of the data. In order to remedy these shortcomings, we devise a new statistic that treats all data on equal footing, without the need to pre-identify specific V_{\max} scales in the data. Application of this new statistic to the existing data on the MW satellite galaxies makes it clear that TBTF is predominantly a statement about the V_{\max} distribution of MW satellites being much broader than predicted by the Λ CDM paradigm.

The paper is organized as follows. In §2 we briefly describe the model and demonstrate that it generates subhalo populations that are indistinguishable from those of large N -body simulations. §3 employs thousands of model realizations to evaluate what fraction of MW-size haloes has subhalo populations consistent with the satellite properties of the Milky Way, using all three formulations of the TBTF problem. In §4 we discuss the severity of TBTF in light of our new statistic, and we summarize our findings in §5.

2 SEMI-ANALYTICAL MODEL

The basis of this work is a semi-analytical model that we developed in Paper I. The model is designed to generate subhalo populations for a target host halo of any mass, in any reasonable Λ CDM cosmology. This section describes the model, and shows that it yields subhalo statistics in excellent agreement with state-of-the-art numerical simulations. However, we start with a brief introduction of halo basics, outlining a number of definitions and notations.

2.1 Halo Basics

Throughout this paper, dark matter haloes at redshift z are defined as spherical systems with a virial radius r_{vir} inside of which the average density is equal to $\Delta_{\text{vir}}(z)\rho_{\text{crit}}(z)$. Here

$\rho_{\text{crit}}(z) = 3H^2(z)/8\pi G$ is the critical density, and $\Delta_{\text{vir}}(z)$ is given by

$$\Delta_{\text{vir}}(z) = 18\pi^2 + 82x - 39x^2 \quad (1)$$

with $x = \Omega_{\text{m}}(z) - 1$ (Bryan & Norman 1998). Haloes whose center falls within the virial radius of another halo are called subhaloes, while haloes that are not subhaloes are called host haloes. The (virial) mass of a host halo is defined as the mass within the virial radius r_{vir} and indicated by M . The mass of a subhalo is defined as the fraction of its mass at accretion (i.e., when it transits from being a host halo to a subhalo) that remains bound, and is indicated by m (see Paper II for an in-depth discussion of subtleties associated with mass definitions).

Throughout we assume that host haloes have a NFW density profile (Navarro, Frenk & White 1997), characterized by a concentration parameter $c = r_{\text{vir}}/r_s$, with r_s the NFW scale radius, and a maximum circular velocity of

$$V_{\text{max}} = 0.465V_{\text{vir}} \sqrt{\frac{c}{\ln(1+c) - c/(1+c)}}, \quad (2)$$

Here

$$V_{\text{vir}} = \sqrt{\frac{GM}{r_{\text{vir}}}} = 159.43 \text{ km s}^{-1} \left(\frac{M}{10^{12} h^{-1} \text{ M}_{\odot}} \right)^{1/3} \times \left[\frac{H(z)}{H_0} \right]^{1/3} \left[\frac{\Delta_{\text{vir}}(z)}{178} \right]^{1/6} \quad (3)$$

is the virial velocity, and the radius, r_{max} , at which the circular velocity reaches its maximum value, is given by

$$r_{\text{max}} = 2.163 r_s. \quad (4)$$

2.2 Model Description

The semi-analytical model that we use to construct realizations of dark matter subhalo populations is a strongly improved and modified version of the model introduced in van den Bosch, Tormen & Giocoli (2005; hereafter vdB05). It treats subhalo mass stripping in an orbit-averaged sense, allowing the construction of thousands of realizations in a manner of minutes. This section gives a brief overview of the model ingredients. A more detailed description can be found in Paper I.

The backbone of our model, as for any other semi-analytical model for the substructure of dark matter haloes (e.g., Taylor & Babul 2001, 2004, 2005a,b; Benson et al. 2002; Taffoni et al. 2003; Oguri & Lee 2004; Zentner & Bullock 2003; Peñarrubia & Benson 2005; Zentner et al. 2005; vdB05; Gan et al. 2010; Yang et al. 2011; Purcell & Zentner 2012), is halo merger trees. These describe the hierarchical mass assembly of dark matter haloes, and therefore yield the masses, m_{acc} , and redshifts, z_{acc} , at which the dark matter subhaloes are accreted into their hosts. We also use the merger trees to compute the concentration parameter, c_{acc} , of the subhalo at accretion. For this we use the fact that halo concentration is tightly correlated with its assembly history (e.g., Wechsler et al. 2002; Ludlow et al. 2013). In particular, we compute c_{acc} using the model of Zhao et al. (2009), according to which

$$c(t) = 4.0 \left(1 + \left[\frac{t}{3.75t_{0.04}} \right]^{8.4} \right)^{1/8} \quad (5)$$

Here $t_{0.04}$ is the time at which the main progenitor of the halo in question assembled 4 percent of its mass at time t , which we compute from our merger tree by tracing the assembly history of the subhalo back in time. Using eqs. (2)–(4), combined with m_{acc} , z_{acc} and c_{acc} , we also compute V_{max} and r_{max} of the subhalo at accretion, which we indicate by V_{acc} and r_{acc} , respectively.

After accretion, a subhalo orbits its host halo, subject to tidal stripping, impulsive heating and dynamical friction. Following vdB05 we model the tidal stripping in an orbit-averaged sense, where the average is taken over all orbital energies, eccentricities and phases. Using a simple toy model, in which it is assumed that over a radial orbital period the subhalo is stripped of all mass outside of the subhalo's tidal radius at the orbit's pericentric distance from the center of the host halo (see Paper I for details), one predicts an orbit-averaged mass loss rate that is well described by

$$\frac{dm}{dt} = \mathcal{A} \frac{m}{\tau_{\text{dyn}}} \left(\frac{m}{M} \right)^{\zeta}, \quad (6)$$

with m , M , and τ_{dyn} the instantaneous subhalo mass, host halo mass, and host halo's dynamical time, respectively. The same functional form was also used by Giocoli, Tormen & van den Bosch (2008) to fit the orbit averaged mass loss rates of dark matter subhaloes in numerical N -body simulations, which yielded $\mathcal{A} = 1.54^{+0.52}_{-0.31}$ and $\zeta = 0.07 \pm 0.03$. Our toy model predicts that $\zeta \simeq 0.04$ and that \mathcal{A} follows a log-normal distribution with median $\bar{\mathcal{A}} \simeq 0.81$ and scatter $\sigma_{\log \mathcal{A}} \simeq 0.17$. This scatter in $\bar{\mathcal{A}}$ is due to the variance in orbital properties (energy and angular momentum) and halo concentrations (of both the host and the subhalo). Given the uncertainties in the parameters derived from the simulations, and the oversimplifications of the toy model, we treat \mathcal{A} and ζ as free parameters. As detailed in Paper I, we tune $\bar{\mathcal{A}}$ and ζ so as to reproduce the subhalo mass functions in the Bolshoi simulation (see §2.3 below). This results in $\bar{\mathcal{A}} = 0.86$ and $\zeta = 0.07$, close to the values suggested by the toy model, and in good agreement with the simulation results of Giocoli et al. (2008). The scatter we keep fixed at $\sigma_{\log \mathcal{A}} = 0.17$. For each individual subhalo in our model, we randomly draw a value for \mathcal{A} from the log-normal, and evolve its mass using Eq. (6).

During its pericentric passage, a subhalo experiences impulsive heating which increases the kinetic energy of its constituent particles. Depending on the amount of energy transferred, the subhalo either expands ('puffs up') while re-establishing virial equilibrium, or is tidally disrupted (typically if the kinetic energy injected exceeds the gravitational binding energy of the subhalo). In our model, a subhalo is disrupted (i.e., removed from the inventory) if its mass $m(t)$ drops below a critical mass

$$m_{\text{dis}} \equiv m_{\text{acc}}(< f_{\text{dis}} r_{\text{s,acc}}), \quad (7)$$

with $m_{\text{acc}}(< r)$ the mass enclosed within radius r at accretion, and $r_{\text{s,acc}}$ the NFW scale radius of the subhalo at accretion. The dependence on $r_{\text{s,acc}}$ assures that subhaloes that are more concentrated at accretion are more resistant to disruption. Using idealized N -body simulations, Hayashi et al. (2003) found that $f_{\text{dis}} \simeq 2$, while both Taylor & Babul (2004) and Zentner et al. (2005) used Eq. (7) to model tidal disruption in their semi-analytical models, but with wildly differing values of $f_{\text{dis}} = 0.1$ and $f_{\text{dis}} = 1.0$, respec-

tively. As detailed in Paper I, tidal disruption in numerical N -body simulation occurs for values of f_{dis} that follow a broad (roughly log-normal) distribution with a median of $f_{\text{dis}} \sim 1.5$ and standard deviation $\sigma_{\log(f_{\text{dis}})} \sim 0.55$. Based on these findings, for each subhalo we draw a value of f_{dis} from a similar log-normal distribution, and disrupt the subhalo whenever its mass drops below m_{dis} . By calibrating the model to reproduce the distribution of retained mass fractions, m/m_{acc} , of the surviving subhaloes in the Bolshoi simulation, we find that we need to introduce a weak mass dependence in f_{dis} , and we end up modeling the f_{dis} distribution as a log-normal with median

$$\bar{f}_{\text{dis}} = 1.5 \left[1 + 0.8 \left| \log \left(\frac{m_{\text{acc}}}{M_{\text{acc}}} \right) \right|^{-3} \right] \quad (8)$$

and standard deviation $\sigma_{\log(f_{\text{dis}})} = 0.55$.

The model for mass stripping and tidal disruption described above regulates the mass evolution of the subhaloes. However, in order to address TBTF, we also need to model the structure (i.e., density distribution) of the individual subhaloes. In particular, we need to be able to predict V_{max} and r_{max} . Based on the idealized simulations of Peñarrubia et al. (2008, 2010), we model V_{max} and r_{max} of the subhaloes using

$$\frac{V_{\text{max}}}{V_{\text{acc}}} = 1.32 \frac{x^{0.3}}{(1+x)^{0.4}}, \quad \frac{r_{\text{max}}}{r_{\text{acc}}} = 0.81 \frac{x^{0.4}}{(1+x)^{-0.3}}, \quad (9)$$

with $x = m/m_{\text{acc}}$; i.e., the evolution of V_{max} and r_{max} of subhaloes depends only on the *amount* of mass loss, but not on *how* that mass was lost (see also Hayashi et al. 2003). As shown in Paper I, Eq. (9) is in good agreement with results from various numerical simulations.

2.3 N-body Simulations

In this paper we use several numerical N -body simulations for comparison with our model predictions. The first is the Bolshoi simulation (Klypin, Trujillo-Gomez & Primack 2011), which follows the evolution of 2048^3 dark matter particles in a box of size $250 h^{-1} \text{Mpc}$ using the Adaptive Refinement Tree (ART) code (Kravtsov, Klypin & Khokhlov 1997) in a flat Λ CDM cosmology with parameters $(\Omega_{\text{m},0}, \Omega_{\Lambda,0}, \Omega_{\text{b},0}, h, \sigma_8, n_s) = (0.27, 0.73, 0.047, 0.7, 0.82, 0.95)$ (hereafter ‘Bolshoi cosmology’). With a particle mass $m_{\text{p}} = 1.4 \times 10^8 h^{-1} \text{M}_{\odot}$, Bolshoi resolves haloes down to $\sim 10^{10} h^{-1} \text{M}_{\odot}$ (corresponding to $V_{\text{max}} \sim 50 \text{ km s}^{-1}$). We use the publicly available halo catalogs[†] obtained using the phase-space halo finder ROCKSTAR (Behroozi et al. 2013a,b). ROCKSTAR haloes are defined as spheres with an average density of $\Delta_{\text{vir}} \rho_{\text{crit}}$, in line with the halo definition used throughout this paper.

In addition to the Bolshoi simulation, we also compare our results to the ELVIS suite of zoom-in simulations of 48 MW-size dark matter haloes (Garrison-Kimmel et al. 2014a). These cover the mass range $11.85 < \log[M/(h^{-1} \text{M}_{\odot})] < 12.31$, comparable to the range of masses quoted for the Milky Way in the literature. The haloes have been selected from medium-resolution cosmological volumes of box size $50 h^{-1} \text{Mpc}$

and re-simulated with progressively higher resolution up to $m_{\text{p}} = 1.35 \times 10^5 h^{-1} \text{M}_{\odot}$. The ELVIS suite adopts a flat Λ CDM cosmology with $(\Omega_{\text{m},0}, \Omega_{\Lambda,0}, \Omega_{\text{b},0}, h, \sigma_8, n_s) = (0.266, 0.734, 0.045, 0.7, 0.801, 0.963)$ (hereafter ‘WMAP7 cosmology’), which are the parameters that best fit the 7-year data release of the Wilkinson Microwave Anisotropy Probe (Larson et al. 2011). The halo catalogs of the ELVIS suite are publicly available[‡], and contain subhaloes (identified with ROCKSTAR), and using the same halo definition as for Bolshoi), down to the resolution limit of $V_{\text{max}} = 8 \text{ km s}^{-1}$.

2.4 Comparison with Simulations

In this section, we first summarize the results of Paper I & II by showing that the model accurately matches the *average* subhalo mass and V_{max} functions extracted from N -body simulations, and then demonstrate that the same model, without any modifications, also accurately reproduces the halo-to-halo variance of subhalo statistics.

The upper panels of Fig. 1 compare the model predictions for the average subhalo mass function, $dN/d \log(m/M_0)$, and the average subhalo velocity function, $dN/d \log(V_{\text{max}}/V_{\text{vir},0})$ (solid and long-dashed curves), with the results from the Bolshoi simulation (filled and open circles). The latter are averaged over a total of 281 host haloes with mass $M_0 = 10^{14.25 \pm 0.25} h^{-1} \text{M}_{\odot}$, while the model predictions are obtained averaging over 2000 realizations of host haloes with mass $M_0 = 10^{14.25} h^{-1} \text{M}_{\odot}$, adopting the Bolshoi cosmology. Solid lines and filled circles indicate the abundances of the surviving subhaloes as a function of their *present-day* mass and V_{max} , while dashed lines and open circles show the abundances of the same subhaloes, but as function of their mass and V_{max} *at accretion*. In both cases, the model predictions are in excellent agreement with the Bolshoi results. Note that the abundance functions *at accretion* are not to be confused with the *unevolved* subhalo mass and/or V_{max} functions, and which are indicated by the short-dashed curves. The latter include *all* subhaloes that have *ever* been accreted onto the main progenitor of the host halo, and includes those subhaloes that have been disrupted since. Note that the unevolved subhalo mass and velocity functions are substantially higher than those for the surviving population, indicating that subhalo disruption is extremely efficient and important.

The lower, left-hand panel of Fig. 1 plots the concentrations at accretion of the present-day, surviving subhaloes as a function of their mass at accretion. The model prediction is again in excellent agreement with Bolshoi, indicating that our model accurately reproduces the structural properties of subhaloes at infall. Finally, the lower, right-hand panel of Fig. 1 compares the distributions of the retained mass fraction, m/m_{acc} , of the present-day, surviving subhaloes. Note that very few subhaloes lose more than 90% of their initial mass, which is another manifestation of efficient subhalo disruption. Here the good agreement between the model and Bolshoi lays the foundation for the accurate model prediction of the parameters that are important for TBTF, V_{max} and r_{max} , whose evolution is purely a function of m/m_{acc} (see Eq. [9])

[†] http://www.slac.stanford.edu/~behroozi/Bolshoi_Catalogs/

[‡] <http://localgroup.ps.uci.edu/elvis/data.html>

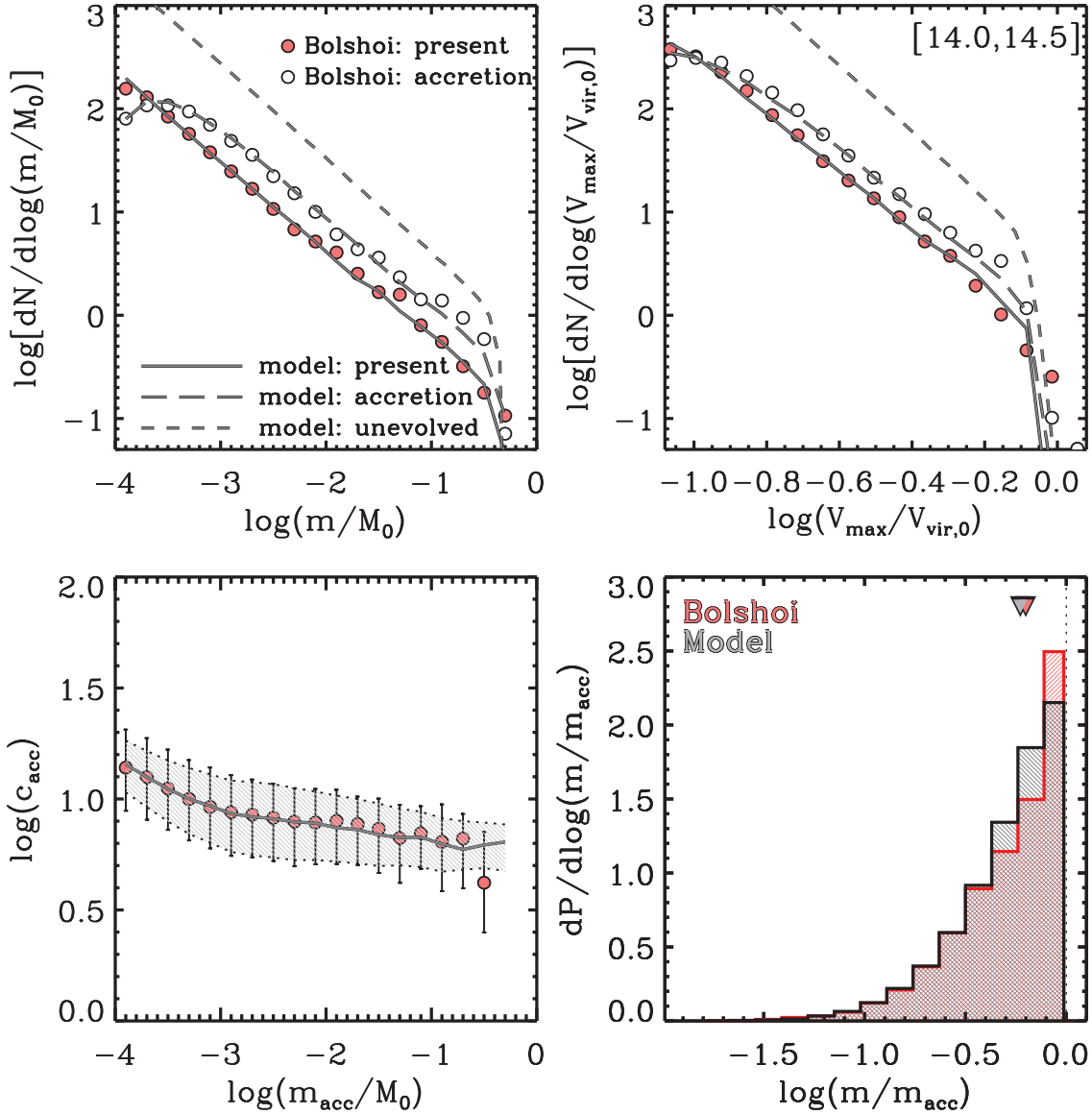


Figure 1. The upper panels compare the average subhalo mass (left) and velocity (right) functions of the Bolshoi simulation (circles) and our model (lines). The line- and symbol- styles differentiate the results for the present-day surviving subhaloes (‘present’), the surviving subhaloes at accretion (‘accretion’), and all subhaloes ever accreted (‘unevolved’). The lower, left-hand panel plots the concentrations of the surviving subhaloes at accretion, c_{acc} , as a function of their masses at accretion (normalized to the present-day host halo mass). Symbols (Bolshoi) and solid curve (model) represent the median relations, while error bars and hatched region indicate the 68% confidence intervals. Finally, the lower, right-hand panel shows the distributions of the retained-mass fractions of the surviving subhaloes, with downward triangles indicating the medians.

The set of comparisons shown in Fig. 1 are the key diagnostics that we used in Paper I to calibrate our model. Note, though, that the comparison is for host haloes with $M_0 \sim 10^{14.25} h^{-1} M_\odot$, far from the mass scale of interest for the TBTF problem. The reason for showing this mass scale is that, in the Bolshoi simulation, it probes a large dynamic range in subhalo mass (down to $m = 10^{-4} M_0$) and a sufficiently large sample size within the simulation box to be able to compute a reliable average mass function. As we have demonstrated in detail in Papers I and II, the same model is equally successful at other mass scales, as far as they have been probed by simulations.

Fig. 2 plots the *individual*, cumulative subhalo velocity

functions, $N(\geq V_{\max})$, for 1986 host haloes with mass $M_0 = 10^{12.10 \pm 0.01} h^{-1} M_\odot$ (left-hand panel) and 441 host haloes with mass $M_0 = 10^{13.50 \pm 0.05} h^{-1} M_\odot$ (right-hand panel) in the Bolshoi simulation, and compares them with 2000 model realizations of halo mass $M_0 = 10^{12.10} h^{-1} M_\odot$, and 500 model realizations of halo mass $M_0 = 10^{13.50} h^{-1} M_\odot$, respectively. The Bolshoi results are plotted down to $V_{\max} = 50 \text{ km s}^{-1}$, which corresponds to roughly 250 particles, the minimum number of particles required to resolve haloes well enough for a reliable estimate of V_{\max} (see Paper II). For the model realizations, we trace subhaloes down to a mass of $10^{-5} M_0$. In the case of host haloes with $M_0 = 10^{12.10} h^{-1} M_\odot$

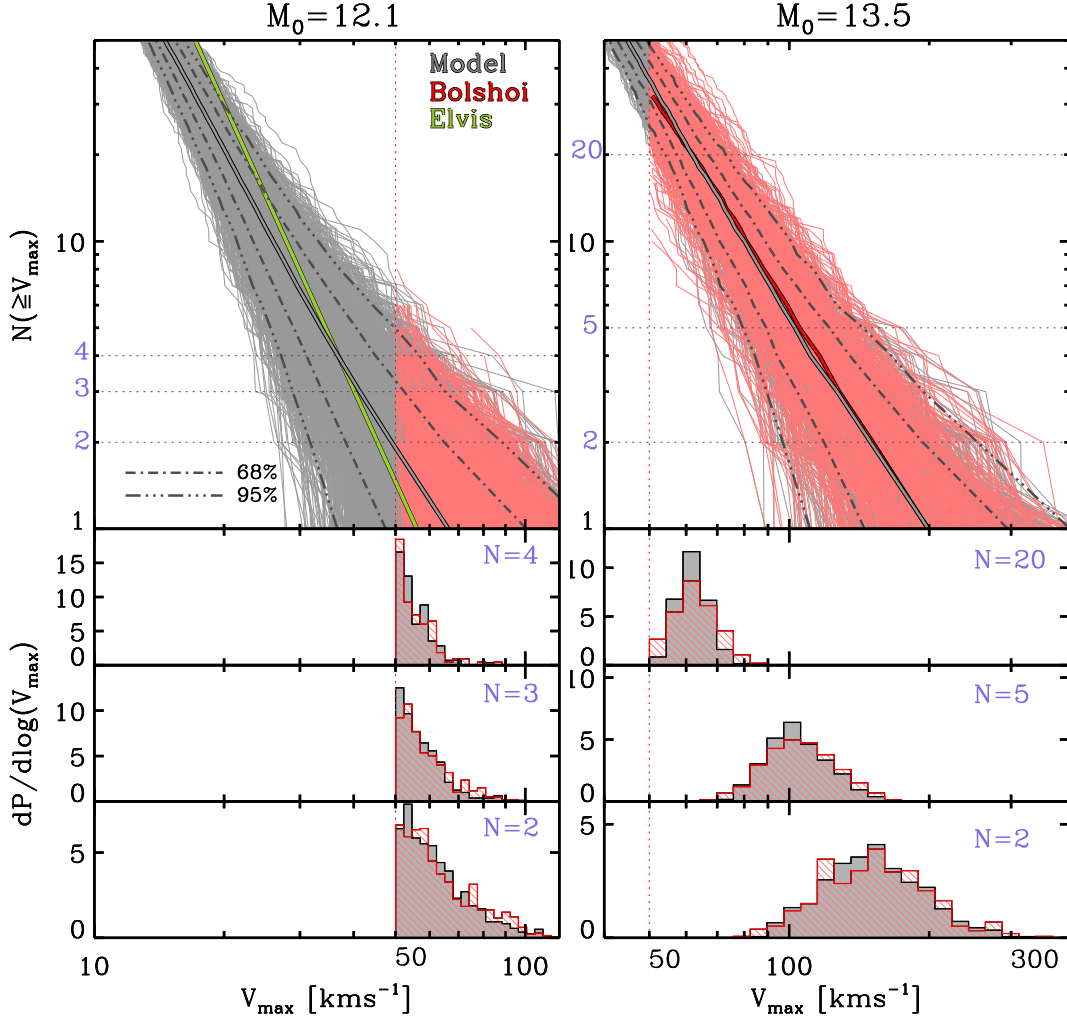


Figure 2. Cumulative subhalo velocity functions for individual host haloes. *Upper, left-hand panel:* 2000 model realizations of haloes with $M_0 = 10^{12.10} h^{-1} M_\odot$ (grey) and 1986 Bolshoi haloes with $M_0 = 10^{12.10 \pm 0.01} h^{-1} M_\odot$ (red). *Upper, right-hand panel:* 500 model realizations of haloes with $M_0 = 10^{13.50} h^{-1} M_\odot$ (grey) and 441 Bolshoi haloes with $M_0 = 10^{13.50 \pm 0.05} h^{-1} M_\odot$ (red). The vertical, dotted lines mark the Bolshoi resolution limit at $V_{\max} = 50 \text{ km s}^{-1}$. The thick, grey line indicates the model’s median V_{\max} at given $N(\geq V_{\max})$, with the dash-dotted lines bracketing the 68% and 95% intervals, as indicated. The thick, red curve (upper, right-hand) is the median relation for the Bolshoi simulation. The thick, green curve (upper, left-hand) is the best-fit median relation for the ELVIS simulation, as given by Garrison-Kimmel et al. (2014a). *Bottom panels:* V_{\max} distribution of the N^{th} subhalo rank-ordered in V_{\max} .

this roughly translates to $V_{\max} = 10 \text{ km s}^{-1}$, which is more than sufficient for a detailed assessment of TBTF.

The model predictions manifest excellent agreement with the Bolshoi results for both mass scales. In the case of $M_0 \sim 10^{13.50} h^{-1} M_\odot$, for which the median in Bolshoi can be measured over an appreciable range in V_{\max} , the ensemble average of the model predictions (indicated by the thick gray line) agrees almost perfectly with that of the Bolshoi simulation data (solid red line). In terms of the halo-to-halo variance, the model and Bolshoi results are almost indistinguishable down to the resolution limit of the simulation. This is nicely illustrated in the bottom panels of Fig. 2, which show the V_{\max} distributions at several values of $N(\geq V_{\max})$, as indicated.

The average, cumulative subhalo velocity functions are usually described by a simple power law, $N(\geq V_{\max}) \propto V_{\max}^{-\alpha}$ (at least for $N \gtrsim 2$). The Bolshoi simulation, against which our model is calibrated, yields a slope of $\alpha \approx 2.9$ with, as far

as we can tell given the limited mass resolution, no dependence on host halo mass (see Papers I & II). This is in excellent agreement with our model predictions, which also yields $\alpha \approx 2.9$ without any significant dependence on host halo mass. The ELVIS suite, however, seems to predict a slope that is significantly steeper, with $\alpha = 3.3$ (Garrison-Kimmel et al. 2014a). It is unclear what the cause is of this discrepancy. We emphasize that most other simulations all suggest that $\alpha \lesssim 3$ (e.g., Klypin et al. 1999; Reed et al. 2005; Madau et al. 2008; Diemand et al. 2008; Wu et al. 2013). The only simulations for which similarly large values for α have been reported are the Millennium-II simulation (Boylan-Kolchin et al. 2009) and the suite of Aquarius simulations (Springel et al. 2008). Both of these were analyzed with the halo finder SUBFIND (Springel, White & Hernquist 2001), which has been shown to give much steeper subhalo mass and velocity functions compared to other halo finders, including ROCKSTAR (see Paper II). Based on these considerations, we

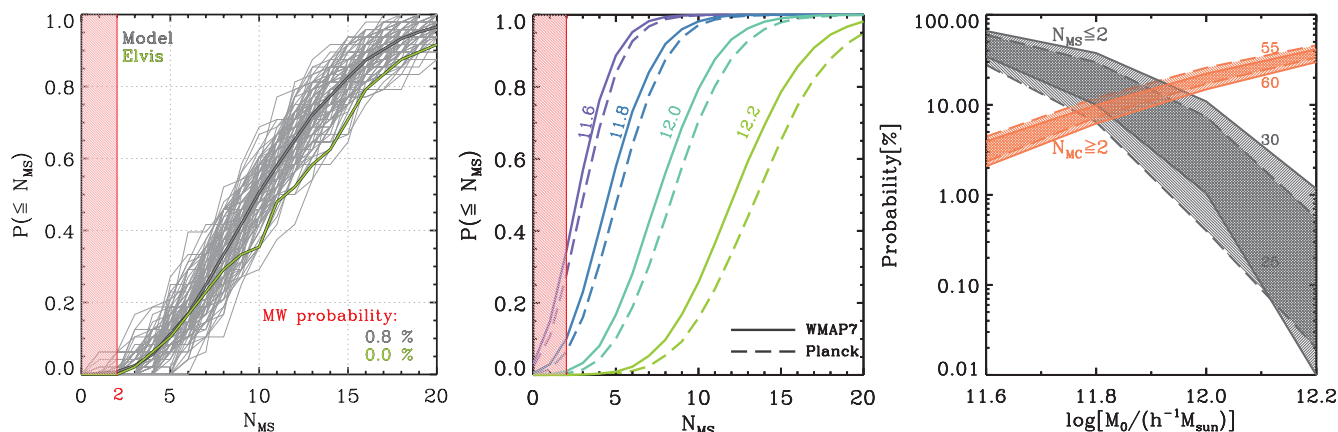


Figure 3. *Left-hand panel:* the fraction of host haloes $\leq N_{\text{MS}}$ massive subhaloes for the 4800 model realizations of ELVIS-size haloes (thick, grey line), the actual ELVIS simulation suite (green), and the 100 mock ELVIS suites (thin, grey lines). Realizations with $N_{\text{MS}} \leq 2$ are considered as MW-consistent. *Middle panel:* same as the left-hand panel, but for 10,000 realizations of different halo masses and cosmologies, as indicated. *Right-hand panel:* the probabilities, i.e., fraction out of 10,000 realizations, of having no more than two massive subhaloes (grey) and no less than two Magellanic-Cloud analogs (orange) as a function of halo mass. The upper and lower bounds of each band correspond to different threshold V_{max} values, as indicated, while solid and dashed curves indicate results for the WMAP7 and Planck cosmologies, respectively.

trust the (current calibration of the) model for the study of MW-size hosts. If future simulations confirm steeper power-law slopes at Galactic mass scales, then it means that some of our model parameters, such as ζ and \bar{A} , must have some mass dependence[§], for which we thus far see no indication in the Bolshoi simulation that covers 2-3 orders of magnitude in host halo mass.

3 ASSESSING THE TOO BIG TO FAIL PROBLEM

In this section, we use the model introduced above to gauge the severity of TBTF in the massive subhaloes formulation (§3.1), the gap formulation (§3.2), and the density formulation (§3.3). We use our model to generate 100 realizations of the ELVIS suite as follows. Adopting the same WMAP7 cosmology as used for the ELVIS simulations, for each halo mass in the ELVIS suite of 48, we generate 100 model realizations with a mass resolution of $m/M_0 = 10^{-5}$. The resulting ensemble of 4800 MW-size host haloes ($M_0 = 10^{12.08 \pm 0.23} h^{-1} M_\odot$) is then split in 100 mock ELVIS suites, each with exactly the same distribution of halo masses. We use this set below to compare our model predictions with those from the ELVIS suite, and to gauge the suite-to-suite variation of the various TBTF statistics. In addition, in order to probe the dependence on halo mass and cosmological parameters, we also construct ensembles of 10,000 model realizations each for several values of M_0 , and for a few different cosmologies.

When comparing model predictions to data, we use the V_{max} values for the MW and its satellites listed in Table 1. These are compiled from Xue et al. (2008), van der Marel & Kallivayalil et al. (2014), Kallivayalil et al. (2013),

Kuhlen (2010), and Boylan-Kolchin et al. (2012). Most of the V_{max} values for the dSphs are taken from Kuhlen (2010) and Boylan-Kolchin et al. (2012). Both studies used similar methodology which we briefly describe in what follows.

The only kinematic information available for the MW dSphs are the line-of-sight velocities of individual stars, which constrain the dynamical mass, $M(< r)$, enclosed within some radius, r , that is typically much smaller than r_{max} (e.g., Strigari et al. 2008; Wolf et al. 2010). In order to infer the corresponding V_{max} , Kuhlen (2010) and Boylan-Kolchin et al. (2012) assign weights to subhaloes in the Via Lactea II and Aquarius simulations, respectively, based on how closely they match the measured $M(< r)$. The corresponding dSph is then assigned the weighted-average V_{max} of these subhaloes. A crucial underlying assumption of this method is that the subhaloes in the zoom-in simulations used are representative of the Λ CDM subhalo populations of MW sized haloes. The validity of this assumption is challenged by the dramatic halo-to-halo variance of subhalo populations. Fortunately, for the few dSphs covered by both Kuhlen (2010) and Boylan-Kolchin et al. (2012), the inferred V_{max} values are mutually consistent within the errors. When available, we use the more recent results of Boylan-Kolchin et al. (2012), since they are based on a larger sample of six host haloes, as compared to only one in the case of Kuhlen (2010).

For the few dwarfs without published V_{max} constraints (Sgr dwarf, Bootes II, Segue II, Bootes I, and Leo V), we use the relation $V_{\text{max}} = 2.2\sigma_{\text{LOS}}$ advocated by Rashkov et al. (2012), and the published stellar line-of-sight velocity dispersion σ_{LOS} (McConnachie 2012 and references therein). The resulting V_{max} values are indicated in brackets in Table 1. Note that we do not include the Canis Major and Bootes III stellar overdensities in this list, as we consider them already disrupted. We emphasize, though, that including them in the inventory of MW satellites has no impact on any of our results and/or conclusions.

[§] For example, we find that with $\zeta = 0.19$ and $\bar{A} = 1.29$ the model accurately reproduces the ELVIS results.

Table 1. Maximum circular velocity of MW and its satellites.

Object	V_{\max} [km s^{-1}]	Reference
Milky Way	170.0 ± 15.0	[1]
LMC	91.7 ± 18.8	[2]
SMC	60.0 ± 5.0	[3]
Sagittarius	(25.1 ± 1.5)	
Bootes II	(23.1 ± 16.3)	
Draco	$20.5^{+4.8}_{-3.9}$	[5]
Ursa Minor	$20.0^{+2.4}_{-2.2}$	[5]
Fornax	17.8 ± 0.7	[5]
Sculptor	$17.3^{+2.2}_{-2.0}$	[5]
Leo I	$16.4^{+2.3}_{-2.0}$	[5]
Ursa Major I	14^{+3}_{-1}	[4]
Ursa Major II	13^{+4}_{-2}	[4]
Leo II	$12.8^{+2.2}_{-1.9}$	[5]
Sextans	$11.8^{+1.0}_{-0.9}$	[5]
Canes Venatici I	$11.8^{+1.3}_{-1.2}$	[5]
Carina	$11.4^{+1.1}_{-1.0}$	[5]
Canes Venatici II	$11^{+2}_{-2.1}$	[4]
Hercules	$11^{+3}_{-1.6}$	[4]
Segue I	$10^{+7}_{-1.6}$	[4]
Coma Berenices	$9.1^{+2.9}_{-0.9}$	[4]
Willman 1	$8.3^{+2.7}_{-0.8}$	[4]
Leo V	$(8.1^{+5.1}_{-3.1})$	
Segue II	$(7.5^{+5.5}_{-2.6})$	
Bootes I	$(5.3^{+2.0}_{-1.1})$	
Leo IV	$5.0^{+2.2}_{-0.8}$	[4]

The references for the values of V_{\max} listed in Column (3) are: [1] Xue et al. (2008); [2] van der Marel & Kallivayalil (2014); [3] Kallivayalil et al. (2013); [4] Kuhlen (2010); and [5] Boylan-Kolchin et al. (2012). Values in brackets are inferred from the empirical relation for MW dSphs, $V_{\max} = 2.2\sigma_{\text{LOS}}$ (Rashkov et al. 2012), with σ_{LOS} measurements from McConnachie (2012) and references therein.

3.1 The Abundance of Massive Subhaloes

The TBTF problem was originally expressed as a tension between the rotation curves of the ~ 10 most massive subhaloes in MW-size host haloes and the kinematics data of the ~ 10 brightest MW dwarf spheroidals (hereafter dSphs). The MW dSphs all have stellar kinematics consistent with $V_{\max} \lesssim 25 \text{ km s}^{-1}$, while the subhaloes have $V_{\max} \gtrsim 25 \text{ km s}^{-1}$. Therefore, several studies have used the abundance of subhaloes with V_{\max} greater than some threshold value (typically in the range of 25-30 km s^{-1}) as a measure of the TBTF severity (e.g., Boylan-Kolchin et al. 2011, 2012; Wang et al. 2012; Garrison-Kimmel et al. 2014b). In particular, Garrison-Kimmel et al. (2014b) define ‘massive failures’ as subhaloes that started out massive ($V_{\text{acc}} > 30 \text{ km s}^{-1}$) and remain massive ($V_{\max} > 25 \text{ km s}^{-1}$) to the present day. The argument is that such subhaloes have potential wells in which galaxy formation is expected to ‘succeed’, to the extent that the absence of a satellite galaxy signals a ‘massive failure’. We refrain from this nomenclature, as it leads to confusion when addressing the LMC and SMC; instead, we simply refer to subhaloes with $V_{\text{acc}} > 30 \text{ km s}^{-1}$ and $V_{\max} > 25 \text{ km s}^{-1}$ as ‘massive subhaloes’.

The left-hand panel of Fig. 3 plots the cumulative dis-

tribution of the number of massive subhaloes, N_{MS} , per host halo, in each of the 100 mock Elvis suites (thin, gray lines). For comparison, the thick, green line shows the results from the actual ELVIS suite. Typically, the N_{MS} distribution is broad, ranging from $N_{\text{MS}} = 0$ to ~ 30 . The median ranges from 8 to 13, which nicely brackets the median of the ELVIS suite, which is 11. The red, vertical line corresponds to $N_{\text{MS}} = 2$ and indicates the number of massive subhaloes around the Milky Way, which correspond to the LMC and SMC. Based on the 4800 model realizations (which sample exactly the same host halo masses as the ELVIS suite), only 0.8% of the MW-sized haloes have no more than two massive subhaloes. The suite-to-suite variance of that percentage ranges from 0% to 6%, indicating that a set of 48 host haloes is insufficient for a meaningful evaluation of the TBTF problem.

3.1.1 Mass and Cosmology Dependence

The middle panel of Fig. 3 plots the cumulative distributions of N_{MS} for four different host halo masses $\log[M_0/(h^{-1} M_{\odot})] = 11.6, 11.8, 12.0$ and 12.2 , and for two different cosmologies; ‘WMAP7’ and ‘Planck’. The latter has $(\Omega_{\text{m},0}, \Omega_{\Lambda,0}, \Omega_{\text{b},0}, h, \sigma_8, n_s) = (0.3175, 0.6711, 0.0486, 0.6825, 0.8344, 0.9624)$, which are the values inferred from the Planck cosmic microwave background data (Planck Collaboration et al. 2014). Each is computed using a sample of 10,000 model realizations. Note how decreasing the mass of the host halo results in a larger fraction of realizations that is consistent with the Milky Way in that $N_{\text{MS}} \leq 2$. Changing the cosmology from ‘WMAP7’ to ‘Planck’ causes a slight reduction in the MW-consistent-fraction. We stress, though, that these probabilities are very sensitive to the exact definition of ‘massive subhalo’. Following Garrison-Kimmel et al. (2014b), in the left and middle panels of Fig. 3 we have defined massive subhaloes as having $V_{\text{acc}} \geq 30 \text{ km s}^{-1}$ and $V_{\max} \geq 25 \text{ km s}^{-1}$. In order to gauge the sensitivity to these exact definitions, we have repeated the inventory of massive subhaloes changing the requirement for the present-day maximum circular velocity to $V_{\max} \geq 30 \text{ km s}^{-1}$. This drastically increases the MW-consistent-fraction, as is evident from the right-hand panel of Fig. 3, which summarizes our results. The gray band indicates the probability $P(N_{\text{MS}} \leq 2)$ as function of halo mass. Solid and dashed lines correspond to the WMAP7 and Planck cosmologies, whereas the upper and lower bounds correspond to defining massive subhaloes as obeying $V_{\max} \geq 30 \text{ km s}^{-1}$ or 25 km s^{-1} , respectively. As is evident, one can boost the MW-consistent-fraction to well over 10% by simply reducing the mass of the MW halo to $< 10^{11.8} h^{-1} M_{\odot}$.

These results are in qualitative agreement with Wang et al. (2012), who, based on an investigation of the Millenium-II simulation, argued that the fraction of host haloes having three or fewer subhaloes with $V_{\max} > 30 \text{ km s}^{-1}$ increases from $\lesssim 5\%$ to $\sim 40\%$ as M_0 decreases from $10^{12.15} h^{-1} M_{\odot}$ to $10^{11.85} h^{-1} M_{\odot}$. Similar results were also reported by Vera-Ciro et al. (2013), who, using a semi-analytical model of galaxy formation find that if the Milky-Way haloes are scaled down to $M_0 = 10^{11.75} h^{-1} M_{\odot}$, the number of satellites brighter than Fornax can be lowered from order of 10 to 2-5.

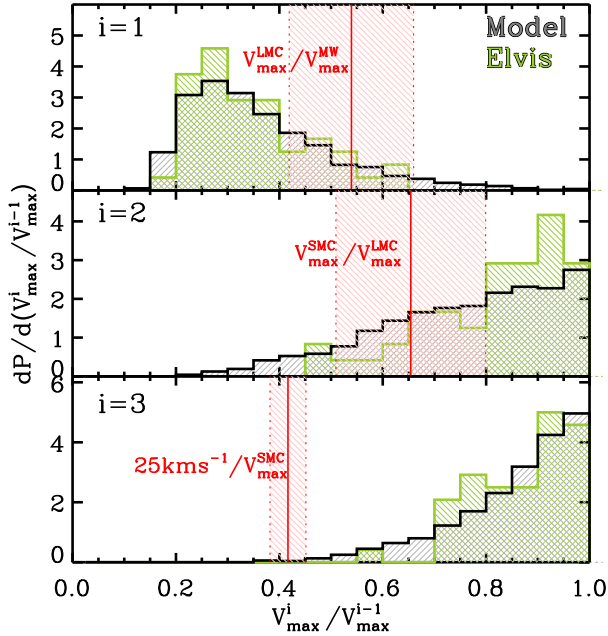


Figure 4. The distributions of the V_{\max} -ratios between the i^{th} and $(i-1)^{\text{th}}$ subhalo (in descending order of V_{\max} , where $i=0$ refers to the host halo itself), for $i=1, 2, 3$ (from top to bottom). The grey distributions are obtained from the 4800 model realizations of the ELVIS-size haloes, and the green histograms are the ELVIS results. The vertical, red lines mark the corresponding MW values, with the red bands indicating the uncertainties due to the errors on the V_{\max} measurements of the MW, LMC and SMC (see Table 1).

To summarize, according to the massive subhalo formulation the TBTF problem can be significantly alleviated by simply lowering the mass of the Milky Way halo to slightly below $10^{12} h^{-1} M_{\odot}$, which is well within current bounds (e.g., Xue et al. 2008; Kafle et al. 2014). However, this alleged solution ignores an important observational fact, namely that the two massive subhaloes of the Milky Way (i.e., the LMC and SMC) actually have fairly large (inferred) values for V_{\max} . According to van der Marel & Kallivayalil et al. (2014) and Kallivayalil et al. (2013), the maximum circular velocity of the LCM and SMC are $91.7 \pm 18.8 \text{ km s}^{-1}$ and $60.0 \pm 5.0 \text{ km s}^{-1}$, respectively. Hence, the MW seems to have two subhaloes with $V_{\max} \gtrsim 60 \text{ km s}^{-1}$. The orange band in the right-hand panel of Fig. 3 shows the probability that the number, N_{MC} , of Magellanic-Cloud-like systems is larger than or equal to two. The latter are defined as subhaloes with $V_{\max} \geq 55 \text{ km s}^{-1}$ (upper solid and dashed curves) or $\geq 60 \text{ km s}^{-1}$ (lower solid and dashed curves). Clearly, the probability $P(N_{\text{MC}} \geq 2)$ decreases with decreasing halo mass. Hence while lowering the mass of the MW halo reduces its abundance of massive subhaloes with $V_{\max} \gtrsim 25 \text{ km s}^{-1}$, it also makes it less likely that they have V_{\max} values in agreement with the Magellanic clouds.

3.2 Gap Statistics

Based on the above findings, the real tension between the Milky Way and a simulated MW-size halo is that the third

most massive satellite has a surprisingly small V_{\max} of $\sim 25 \text{ km s}^{-1}$ (irrespective of whether this third system is Draco, Ursa Minor, Fornax or the Sgr dwarf) compared to that of its second most massive satellite, the SMC, which seems to have $V_{\max} \sim 60 \text{ km s}^{-1}$. Therefore, a more specific formulation of the TBTF problem is the existence of a V_{\max} gap between the second and the third most massive MW satellites.

Fig. 4 plots the distributions of the V_{\max} ratio between the i^{th} and $(i-1)^{\text{th}}$ subhaloes, rank-ordered by V_{\max} , for $i=1, 2$, and 3. Here the 0^{th} subhalo corresponds to the host halo itself. The model predictions for the 100 mock ELVIS suites and the actual ELVIS simulation results are in excellent agreement for all three cases. We take the model distributions as benchmarks to gauge how (a) typical the MW halo is. Using the V_{\max} values listed in Table 1, the ratio of the first subhalo to the host halo, $V_{\max}^{1\text{st}}/V_{\max}^{0\text{th}}$, for the MW is 0.54 ± 0.12 (indicated as the vertical, hatched band in the upper panel of Fig. 4), well within the theoretical range. Similarly, the V_{\max} -ratio of the second to first ranked subhalo (middle panel) for the MW is 0.65 ± 0.14 , again in good agreement with the theoretical predictions. Hence, it is clear that the subhaloes that host the two Magellanic clouds are perfectly common. The TBTF problem is revealed in the third panel: assuming $V_{\max} = 25 \text{ km s}^{-1}$ for the third MW satellite, and the aforementioned V_{\max} measurement for the SMC, the V_{\max} -ratio for $i=3$ for the MW is 0.42 ± 0.04 , which is small compared to the model prediction whose 95 percent confidence interval ranges from 0.56 to 0.99.

Interestingly, the $V_{\max}^{3\text{rd}}/V_{\max}^{2\text{nd}}$ -distribution predicted by the model extends down to values well below that of the MW, indicating that it is possible, albeit rare, for dark matter haloes to reveal a V_{\max} -gap comparable to that in the MW. To make this more quantitative, we construct an ensemble of 10,000 model realizations for $M_0 = 10^{11.8} h^{-1} M_{\odot}$ in the WMAP7 cosmology and identify realizations with $V_{\max}^{3\text{rd}} \leq 25 \text{ km s}^{-1}$ and $V_{\max}^{2\text{nd}} \geq 55 \text{ km s}^{-1}$. Among the 10,000 realizations, we only find 6 (0.06%) that meet these criteria[¶]. The left-hand panel of Fig. 5 compares the cumulative subhalo velocity functions for these six MW-consistent cases (solid lines) with that of the actual MW satellites (red symbols with error-bars; data taken from Table 1). Note that three of the six model realizations mimic the MW extremely well down to $V_{\max} \sim 15 \text{ km s}^{-1}$. For smaller V_{\max} all models predict far more satellites than observed. We emphasize though, that the inventory of MW satellites is incomplete at the low V_{\max} end. Tollerud et al. (2008) have demonstrated that the luminosity function of MW satellites suffers from incompleteness for $M_V \gtrsim -9$ ^{||}. Since there are ten MW satellites brighter than this, we estimate that the MW inventory is roughly complete down to $V_{\max} \sim 15 \text{ km s}^{-1}$. Although we acknowledge that the rank-order in M_V is not equal to that in V_{\max} , we argue that the discrepancy between model and data for $V_{\max} < 15 \text{ km s}^{-1}$ is most likely a manifestation of incompleteness in the data.

The right-hand panels of Fig. 5 plot the circular velocity

[¶] We also repeated this exercise for host haloes with $M_0 = 10^{12.0} h^{-1} M_{\odot}$, which resulted in only a single candidate.

^{||} The eight new MW dwarfs recently discovered in the Dark Energy Survey (DES Collaboration et al. 2015) are indeed all much fainter than this).

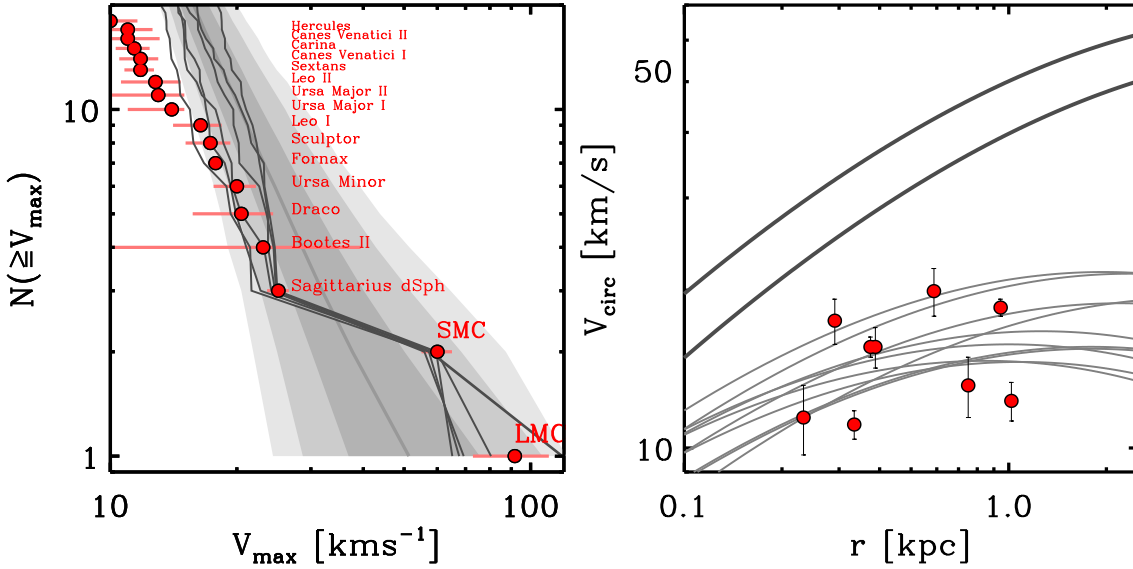


Figure 5. Rare model realizations with a V_{\max} gap consistent with that observed in the MW. *Left-hand panel:* grey, solid lines show the cumulative V_{\max} functions for the only six realizations (out of 10,000 haloes with $M_0 = 10^{11.8} h^{-1} M_{\odot}$) that reveal a MW-consistent V_{\max} gap. For comparison, the solid circles with error bars show the actual MW data (see Table 1). The median, and the 68, 95, and 99.7 percentiles of the 10,000 model realizations are indicated in a shaded background with progressively lighter grey. *Right-hand panel:* the rotation curves of the first 12 subhaloes with the highest V_{\max} values in one of those six realizations (the other five cases look very similar). The two rotation curves with a thicker line-style indicate the Magellanic-Cloud analogs, while symbols with error bars represent the nine brightest MW dSphs (data taken from Wolf et al. 2010).

curves for the 12 subhaloes with the largest V_{\max} in one of our model realizations, randomly chosen from the set of six shown in the left-hand panel (results for the other 5 are similar). Following Garrison-Kimmel et al. (2014b), these circular velocity profiles are computed using the V_{\max} and r_{\max} values for each subhalo as predicted by the model (see §2.2), and assuming that subhaloes follow an Einasto profile (Einasto 1965)

$$\rho(r) = \rho_{-2} \exp \left[\frac{-2}{\alpha} \left\{ \left(\frac{r}{r_{-2}} \right)^{\alpha} - 1 \right\} \right] \quad (10)$$

where r_{-2} is the radius at which the logarithmic slope of the density distribution is equal to -2 , $\rho_{-2} = \rho(r_{-2})$ and α is a shape parameter. In computing our model circular velocity curves we have adopted $\alpha = 0.18$, which is the typical value for subhaloes in the Aquarius simulation (Springel et al. 2008) ******. For comparison, the red circles with error-bars indicate the circular velocity measurements at the half-light radius, $V_{\text{circ}}(r_{1/2})$, of the 9 brightest MW dSphs (Wolf et al. 2010). Note how this model predicts two Magellanic cloud analogs, with $V_{\max} = 68 \text{ km s}^{-1}$ and 57 km s^{-1} respectively, whose circular velocity curves clearly stand out, with a pronounced gap to the subsequent subhaloes. Note also how the circular velocity curves of these subsequent subhaloes are statistically consistent with the data for the MW dSphs.

Hence, based on the gap statistics, we conclude that,

****** Subhaloes in the Aquarius simulation cover the range $0.15 < \alpha < 0.30$. Note of our results change significantly if we vary α over this range.

within the Λ CDM paradigm, one can find MW-sized haloes with subhalo statistics in excellent agreement with our best current understanding of the Milky Way. However, such haloes seem to be extremely rare. In order to quantify this in more detail, we now investigate the gap statistic in more detail, and as function of host halo mass.

3.2.1 Dependence on Host Halo Mass

The left-hand panel of Fig. 6 plots the cumulative distributions of $N_{\text{gap}} \equiv N_l - N_u$. Here N_l and N_u are the numbers of subhaloes with V_{\max} larger than some *lower* and *upper* limit, respectively. For the solid lines we set these lower and upper limits to be 25 km s^{-1} and 55 km s^{-1} , respectively. Thus defined, N_{gap} is the number of subhaloes in the range $25 \text{ km s}^{-1} < V_{\max} < 55 \text{ km s}^{-1}$. Different colors correspond to different host halo masses, as indicated. For each host halo, we compute $P(\leq N_{\text{gap}})$ using 10,000 model realizations for a WMAP7 cosmology. Taking the best-fit values for V_{\max} of each MW satellite galaxy, as listed in Table 1, and ignoring their uncertainties, the Milky Way has $N_{\text{gap}} = 1$ (the Sgr dSph, for which $V_{\max} = 25.1 \text{ km s}^{-1}$). As is evident from the left-hand panel of Fig. 6, the probability that a Λ CDM halo has $N_{\text{gap}} \leq 1$ is extremely small if $M_0 \gtrsim 10^{12} h^{-1} M_{\odot}$, but rapidly increases with decreasing M_0 . This is quantified more clearly by the solid, black line in the right-hand panel of Fig. 6 which plots $P(N_{\text{gap}} \leq 1)$ as function of host halo mass. We emphasize, though, that these results are very sensitive to how exactly one defines the gap. Setting the lower and upper limits of the gap to 30 km s^{-1} and 60 km s^{-1} , for

example, results in the dashed curves, for which $P(N_{\text{gap}} \leq 1)$ is significantly larger.

The orange, hatched area in the right-hand panel indicates the probability $P(N_u \geq 2)$, where the upper limit corresponds to $V_{\text{max}} = 55 \text{ km s}^{-1}$ (solid line) or 60 km s^{-1} (dashed line), respectively. Note that the probability to host two subhaloes consistent with the two Magellanic Clouds drops below one percent for $M_0 \lesssim 10^{11.4} h^{-1} M_\odot$. Hence, to be consistent with the MW requires that $N_{\text{gap}} \leq 1$ and $N_u \geq 2$. The probability that both constraints are satisfied is indicated by the red band in the right-hand panel, which plots $P(N_{\text{gap}} \leq 1, N_u \geq 2)$ as function of halo mass.

The dashed lines correspond to a different choice for the lower and upper limits of 30 km s^{-1} and 60 km s^{-1} , respectively. Note how the dashed curves are shifted to the left compared to the solid curves, indicating that the typical N_{gap} is significantly smaller for this definition of the $V_{\text{max-gap}}$. Although not shown here, we have verified that changing cosmology from WMAP7 to Planck has weak influence on $P(N_{\text{gap}} \leq 1)$ and $P(N_u \geq 2)$, similar to that shown in Fig. 3, and negligible effect on $P(N_{\text{gap}} \leq 1, N_u \geq 2)$.

The gap statistic reveals a stronger tension than the massive-subhalo count. In particular, at best $\sim 1\%$ of ΛCDM haloes have a $V_{\text{max-gap}}$ comparable to that of the MW, and that is for a MW host halo mass of $M_0 \simeq 10^{11.8} h^{-1} M_\odot$. This probability drops to below 0.1% for $M_0 \lesssim 10^{11.2} h^{-1} M_\odot$ and $M_0 \gtrsim 10^{12.2} h^{-1} M_\odot$. These results are in excellent agreement with the empirical extrapolations of N -body simulation results by Cautun et al. (2014b).

3.3 Density of Massive Subhaloes

The third formulation of TBTF, the one used in the paper by Boylan-Kolchin et al. (2011) that introduced the TBTF problem, is that the most massive subhaloes in simulations are too dense to be consistent with constraints on the MW dSphs. Here the internal densities of satellites are usually characterized in terms of their r_{max} and V_{max} values.

Measurements of the stellar kinematics of satellite galaxies can put accurate constraint on their enclosed mass within their half-light radius (Wolf et al. 2010). These in turn, constrain a degenerate combination of r_{max} and V_{max} (e.g., Zentner & Bullock 2003; Boylan-Kolchin et al. 2011). This motivated PZ12 to define a density proxy, Γ , as a linear combination of $\log(r_{\text{max}})$ and $\log(V_{\text{max}})$;

$$\Gamma \equiv 1 + \log(0.0014 V_{\text{max}}^{2.2} / r_{\text{max}}), \quad (11)$$

which increases in a direction approximately orthogonal to the envelop of the constraint on MW dSphs in the $\log(r_{\text{max}})$ - $\log(V_{\text{max}})$ plane. Thus defined, $\Gamma = 1$ corresponds to the 2σ upper bound of the region in the r_{max} - V_{max} space that is occupied with MW dSphs. A host halo is said to be MW-consistent if *all* its subhaloes obey $\Gamma \leq 1$, while the presence of one or more subhaloes with $\Gamma > 1$ constitutes a manifestation of TBTF.

The upper left-hand panel of Fig. 7 plots the subhaloes in the r_{max} - V_{max} space for the 4800 model realizations of our 100 mock ELVIS suites, color-coded according to their value for V_{acc} . The upper right-hand panel shows the same, but this time for the actual subhaloes in the ELVIS simulation suite of 48 MW-size host haloes. Filled circles indicate the median r_{max} as a function of V_{max} , with error-bars indicating

the 16 and 84 percentiles. Red, dashed lines indicate the loci of $\Gamma = 0, 1$ and 2 . The model predictions are in good agreement with the ELVIS simulation results, in that both predict a median $r_{\text{max}} - V_{\text{max}}$ relation corresponding to $\Gamma > 1$ for $V_{\text{max}} \gtrsim 45 \text{ km s}^{-1}$. Note that all observed MW dwarf spheroidals fall in the range $0 < \Gamma < 1$ (see PZ12).

Following Garrison-Kimmel et al. (2014b), we fit the median $R_{\text{max}} - V_{\text{max}}$ relation with a simple power law

$$\frac{r_{\text{max}}}{1 \text{ kpc}} = A \left(\frac{V_{\text{max}}}{10 \text{ km s}^{-1}} \right)^p. \quad (12)$$

For the model predictions we find $(A, p) = (0.77, 1.37)$, in good agreement with the ELVIS results, for which $(A, p) = (0.73, 1.47)$. A comparison of the best-fit $r_{\text{max}} - V_{\text{max}}$ relations of our model, the ELVIS simulation, and the PZ12 model is shown in the lower left-hand panel of Fig. 7. The PZ12 model $\dagger\dagger$ predicts significantly larger scatter and a much shallower slope ($p = 0.92$) compared to both our model and the ELVIS simulation.

The lower right-hand panel of Fig. 7 plots the cumulative distributions of $\Gamma_{\text{max}} = \max\{\Gamma_i\}$, where the maximum is taken over all subhaloes in a single host halo. In the ELVIS suite, only one out of the 48 host haloes (corresponding to 2.1%) has $\Gamma_{\text{max}} \leq 1$, and is therefore MW-consistent. This is in good agreement with our model predictions, for which we find (using a sample of 4800 host haloes) a MW-consistent fraction of 2.8%. As in §3.1, we can use the 100 mock ELVIS suites to infer the suite-to-suite variance. The median Γ_{max} ranges from 1.1 to 1.3, with a MW-consistent fraction that varies from 0% to 15%. This is another demonstration that the sample size of the ELVIS suite is insufficient for an accurate assessment of TBTF.

As is evident from the lower right-hand panel of Fig. 7, the PZ12 model predicts a Γ_{max} -distribution that is much broader than what is found in the ELVIS simulation suite or predicted by our model. The relatively large difference between PZ12 and our model is most likely due to two reasons. First, PZ12 construct their merger trees using the Somerville & Kolatt (1999) algorithm, which is known to overpredict merger rates, and result in a halo-to-halo variance of mass assembly histories that is too large (e.g., Zhang et al. 2008; Jiang & van den Bosch 2014a). Our model, instead, relies on the Parkinson, Cole & Helly (2008) algorithm, which yields merger trees that are statistically indistinguishable from those extracted from numerical simulations. Second, PZ12 use a different model for evolving V_{max} and r_{max} of subhaloes. In particular, whereas we use Eq.(9) to compute V_{max} and r_{max} , PZ12 simply assume that $V_{\text{max}} \propto m^{1/3}$ and compute r_{max} assuming that dark matter subhaloes follow an NFW profile. Based on a number of tests, we conclude that this PZ12 model for computing the structural parameters of their subhaloes results in a median $r_{\text{max}} - V_{\text{max}}$ relation that is too shallow, while their merger trees are responsible for introducing a scatter in the $r_{\text{max}} - V_{\text{max}}$ relation that is too large, which in turn results in a MW-consistent fraction that is too high.

We caution that the observational constraint on V_{max}

$\dagger\dagger$ The PZ12 predictions are read off from their published figures, which are based on 10,000 realizations of $10^{12} h^{-1} M_\odot$ haloes in a WMAP7 cosmology.

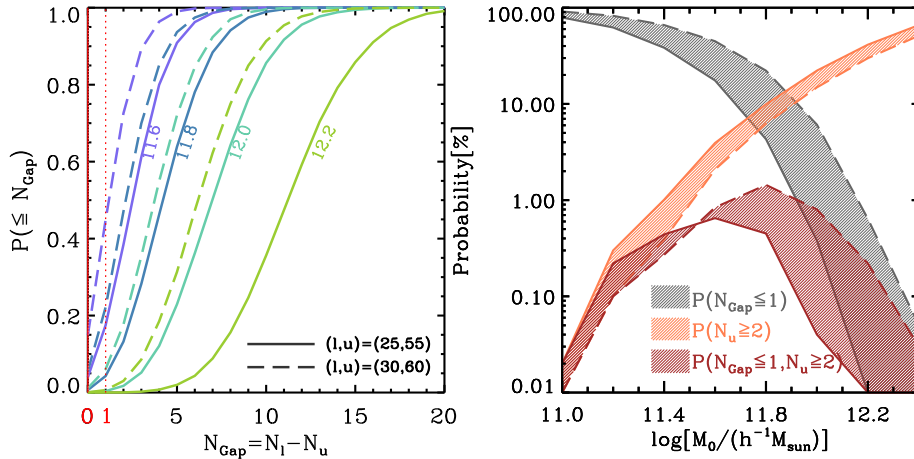


Figure 6. *Left-hand panel:* the fraction of model realizations with no more than N_{Gap} subhaloes with $V_{\text{max}} \in (25, 55) \text{ km s}^{-1}$ (solid lines) or $V_{\text{max}} \in (30, 60) \text{ km s}^{-1}$ (dashed lines), for different host halo masses as indicated (value reflects $\log[M_0/(h^{-1}M_\odot)]$). *Right-hand panel:* the probabilities of having no more than one subhalo in the V_{max} gap, $P(N_{\text{Gap}} \leq 1)$, no less than two Magellanic-Cloud analogs, $P(N_u \geq 2)$, and both $N_{\text{Gap}} \leq 1$ and $N_u \geq 2$, $P(N_{\text{Gap}} \leq 1, N_u \geq 2)$, as a function of host halo mass. The solid and dashed curves correspond to different threshold V_{max} values, as indicated in the left-hand panel.

and r_{max} , expressed as $0 < \Gamma < 1$, is based on the assumption that dark matter subhaloes have NFW density profiles. Vera-Ciro et al. (2013) have shown that if one instead assumes an Einasto profile with $\alpha = 0.5$, the constraints on V_{max} and r_{max} are significantly altered, to the extent that even the densest subhaloes in the Aquarius simulations are now consistent with the data (i.e., one would no longer infer a TBTF problem). However, subhaloes in numerical simulations typically have density profiles that are well fit by an Einasto profile, but with $\alpha \sim 0.2$, for which the constraints on V_{max} and r_{max} are very similar to those obtained assuming an NFW profile. Hence, the constraint $0 < \Gamma < 1$ proposed by PZ12 is still valid, despite the oversimplified assumption that subhaloes follow an NFW profile.

3.3.1 Mass and Cosmology Dependence

Fig. 8 investigates the dependence of the cumulative Γ_{max} distribution on halo mass and cosmology. The left-hand panel plots the results for the WMAP7 cosmology. The fraction of realizations with $\Gamma_{\text{max}} < 1$ increases from 1% at $M_0 = 10^{12.2} h^{-1}M_\odot$ to 29% at $M_0 = 10^{11.6} h^{-1}M_\odot$. Also based on the WMAP7 cosmology, the PZ12 model predicts the MW-consistent fractions to be 20%, 10% and 10% for $M_0 = 10^{11.8} h^{-1}M_\odot$, $10^{12.0} h^{-1}M_\odot$, and $10^{12.2} h^{-1}M_\odot$ respectively, significantly higher than our findings of 16%, 4.5%, and 0.6%.

The middle panel of Fig. 8 plots the same results but now for the Planck cosmology. The MW-consistent fraction increases from 0.1% at $M_0 = 10^{12.2} h^{-1}M_\odot$ to 9% at $M_0 = 10^{11.6} h^{-1}M_\odot$, significantly smaller than for the WMAP7 cosmology. Therefore, a relatively small change in cosmological parameters seems to have a relatively large impact on the TBTF-statistics in the density formulation.

Polisensky and Ricotti (2014) argued that the cosmology dependence mainly manifests itself as a change in the r_{max} of subhaloes. To test this, the right-hand panel of Fig. 8

plots the $r_{\text{max}}-V_{\text{max}}$ diagram for the WMAP7 and Planck cosmologies, at fixed halo mass of $M_0 = 10^{12.0} h^{-1}M_\odot$. In both cases, the $r_{\text{max}}-V_{\text{max}}$ relations are well fit by Eq. (12) with $p \simeq 1.4$. The normalizations of the best-fit relations, though, are different, with $A = 0.62$ for the Planck cosmology, and $A = 0.74$ for the WMAP7 cosmology. This indicates that subhaloes in the Planck cosmology are, on average, ~ 20 percent denser than in the WMAP7 cosmology. The top and side panels of the right-hand panel of Fig. 8 show the average subhalo V_{max} and r_{max} distributions for all subhaloes with $V_{\text{max}} > 18 \text{ km s}^{-1}$, respectively. This clearly shows that the difference in cosmology predominantly manifests itself as a change in the r_{max} distribution of subhaloes, confirming the results of Polisensky and Ricotti (2014).

The cosmology dependence of subhalo densities arises from the cosmology dependence of the host halo assembly histories: larger $\Omega_{\text{m},0}$, smaller $\Omega_{\Lambda,0}$ and larger σ_8 , as in the case of the Planck cosmology compared to the WMAP7 cosmology, all result in earlier (average) formation times for host haloes of given present-day mass (e.g., van den Bosch 2002; Giocoli, Tormen & Sheth 2012). Earlier assembly implies that the host halo accreted its subhaloes at earlier epochs, when the Universe (and therefore the dark matter haloes) was denser.

4 AN ALTERNATIVE STATISTIC

In the previous section we have used three different statistics that have been used in the literature to assess the TBTF problem. If we adopt a MW host halo mass of $M_0 = 10^{12} h^{-1}M_\odot$, the inference is that the MW-consistent fraction ranges anywhere between $\sim 0.1\%$ and $\sim 10\%$, depending on which statistic one uses. Obviously, this raises the question which is the more meaningful statistic to use. We believe the answer is basically none of the above, and the reason is that they either suffer from the "look-elsewhere

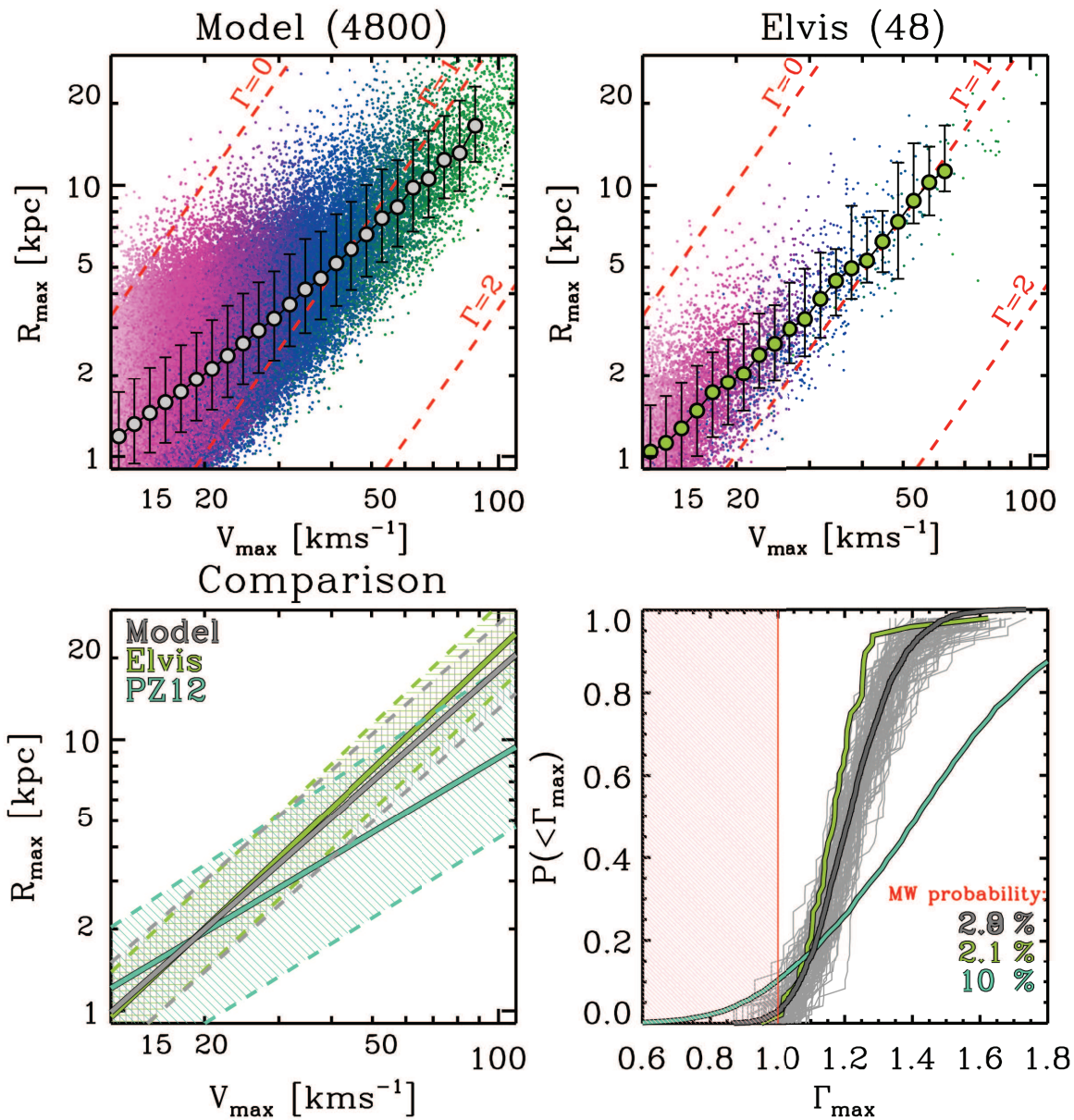


Figure 7. Distribution of subhaloes in r_{\max} - V_{\max} space, for the 4800 model realizations of ELVIS-size haloes (*upper, left-hand panel*) and the 48 ELVIS haloes (*upper, right-hand panel*). Individual dots are subhaloes, color coded by V_{acc} . Circles indicate the median r_{\max} at given V_{\max} bins, with error bars indicating the 16 and 84 percentiles. The red dashed lines are the loci of $\Gamma = 0, 1$, and 2 [Eq.(11)], with $0 < \Gamma < 1$ encompassing the region occupied by MW dSphs. *Lower, left-hand panel:* comparison of the best-fit r_{\max} - V_{\max} relations of our model (grey), the ELVIS simulation (green), and the PZ12 model (cyan), with solid and dashed lines indicating the median relations and the 16 and 84 percentiles respectively. *Lower, right-hand panel:* corresponding cumulative Γ_{\max} distributions. The red-shaded region corresponds to $\Gamma_{\max} < 1$ and is considered ‘MW consistent’.

effect” (e.g., Gross & Vitells 2010), and/or disregard certain aspects of the data.

Both the massive subhaloes formulation and the gap formulation use statistics that require the identification of one or more particular values of V_{\max} ; the massive subhaloes formulation considers the number of subhaloes with V_{\max} above some limit, while the gap statistic is based on

the number of satellites between two values of V_{\max} . These values are chosen by the user after carefully examining the data on the MW, in an attempt to find a statistic for which the MW is least likely. This is a clear example of the look-elsewhere effect. For example, if the MW satellite system would have revealed a V_{\max} -gap between 10 km s^{-1} and 30 km s^{-1} , rather than between 25 km s^{-1} and 55 km s^{-1} ,

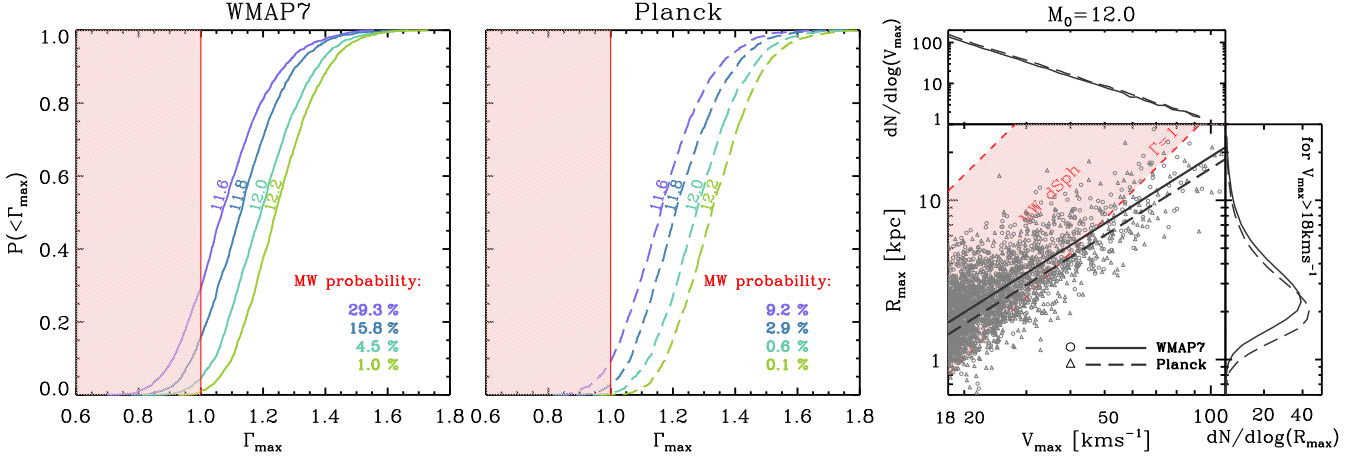


Figure 8. Cumulative Γ_{\max} distributions for different halo masses, in the WMAP7 cosmology (left-hand panel), and the Planck cosmology (middle panel). The MW-consistent regime ($\Gamma_{\max} < 1$) is highlighted in red. The right-hand panel shows the subhalo r_{\max} – V_{\max} relations for a host halo mass $M_0 = 10^{12.0} h^{-1} M_{\odot}$ in the WMAP7 and Planck cosmologies. The circles (WMAP7) and triangles (Planck) correspond to a random subsample of model realizations, while the solid and dashed lines indicate the corresponding median relations. The red shaded band indicates the region occupied by MW dSphs. The top and side panels plot the V_{\max} and r_{\max} distributions for model subhaloes with $V_{\max} > 18 \text{ km s}^{-1}$. Note that subhaloes are expected to be significantly denser (i.e., smaller r_{\max}) in the Planck cosmology.

this would have raised a similar concern of being inconsistent with Λ CDM predictions. Yet, such a gap does not manifest itself based on the gap statistic used above to assess TBTF. Hence, rather than asking what the probability is for a gap between 25 km s^{-1} and 55 km s^{-1} , one should ponder about the probability that a host halo reveals *some* gap, not necessarily between these two exact values. This is also evident from the fact that we have demonstrated that small changes in the ‘user-specified’ values that define the gap results in large changes in the MW consistent fraction, and thus in the inference regarding the severity of TBTF. Ideally, then, one should use a statistic that is ‘blind’ in that it does not rely on an examination of the data beforehand.

Another problem with the previous statistics is that both the massive subhaloes formulation and the density formulation do not properly account for the Magellanic clouds. We believe this to be a serious shortcoming, as the Magellanic clouds, by themselves, put a tight constraint on the mass of the Milky Way host halo (e.g., Busha et al. 2011).

Finally, it is important to realize that no study of TBTF to date has properly accounted for the observational errors in the V_{\max} measurements of the MW satellite galaxies. As we demonstrate below, this introduces a huge uncertainty on any MW-consistent fraction, and should be properly taken into account.

Based on these considerations, we devise a new statistic that is ‘blind’ (i.e., no scale has to be picked upfront), uses all data on equal footing, and allows for a straightforward treatment of errors in the V_{\max} measurements of individual MW satellites. Consider two rank-ordered distributions, $\mathcal{S}_1(x_1, x_2, \dots, x_N)$ and $\mathcal{S}_2(y_1, y_2, \dots, y_N)$. In our application, x_i and y_i are the V_{\max} values of dark matter subhaloes, while \mathcal{S}_1 and \mathcal{S}_2 are two different host haloes (i.e., two different model realizations for a host halo of given mass, or a model realizations plus the actual V_{\max} data for satellite galaxies in the MW). Note that \mathcal{S}_1 and \mathcal{S}_2 have the same number of elements and that $x_{i+1} \geq x_i$ and $y_{i+1} \geq y_i$. We now introduce the statistic

$$Q \equiv \frac{\sum_{i=1}^N |x_i - y_i|}{\sum_{i=1}^N (x_i + y_i)} \quad (13)$$

which is a measure for the difference between the (cumulative) distributions of \mathcal{S}_1 and \mathcal{S}_2 . In particular, $\frac{1}{N} \sum_{i=1}^N |x_i - y_i|$ is the absolute value of the area between the cumulative distributions of \mathcal{S}_1 and \mathcal{S}_2 . We normalize this area by $\frac{1}{N} \sum_{i=1}^N (x_i + y_i)$ so that Q is dimensionless, and insensitive to an overall shift in x and y (i.e., multiplying x_i and y_i by some factor f leaves Q invariant). Note that $Q = 0$ if $\mathcal{S}_1 = \mathcal{S}_2$ (the distributions are identical), while $Q = 1$ if either \mathcal{S}_1 or \mathcal{S}_2 consists solely of null elements (i.e., $x_i = 0$ or $y_i = 0$ for all $i = 1, 2, \dots, N$). Note that this Q -statistic is similar to the Kolmogorov-Smirnov test, which measures the maximum value of the absolute difference, d_{KS} , between two cumulative distributions. However, the KS-test is not well suited to characterize differences in the tails of two distributions; it mainly is sensitive to finding differences in the median. We therefore opted to use the statistic Q instead, which has equal sensitivity throughout the distributions. In adopting Q to assess TBTF, each individual dark matter host halo has a corresponding distribution \mathcal{S} , in which the elements are the rank-ordered values of V_{\max} for the N subhaloes with the largest V_{\max} values.

In order to turn the Q statistic into a probability measure, we proceed as follows. Given $K = 10,000$ model realizations, for a given host halo mass, M_0 , and a given cosmology, we first compute the values Q_{ij} for each pair $\{\mathcal{S}_i, \mathcal{S}_j\}$ (with $i, j = 1, 2, \dots, K$), where \mathcal{S}_i is the rank-ordered distribution of the N largest V_{\max} values for model realization i . Next we compute the average

$$\bar{Q}_i = \frac{1}{K-1} \sum_{j \neq i} Q_{ij} \quad (14)$$

for each of the 10,000 realizations. Finally, we compute the K values of $Q_{\text{MW},i}$ by comparing the V_{\max} distribution of the MW to that of each of the 10,000 model realizations, which yields

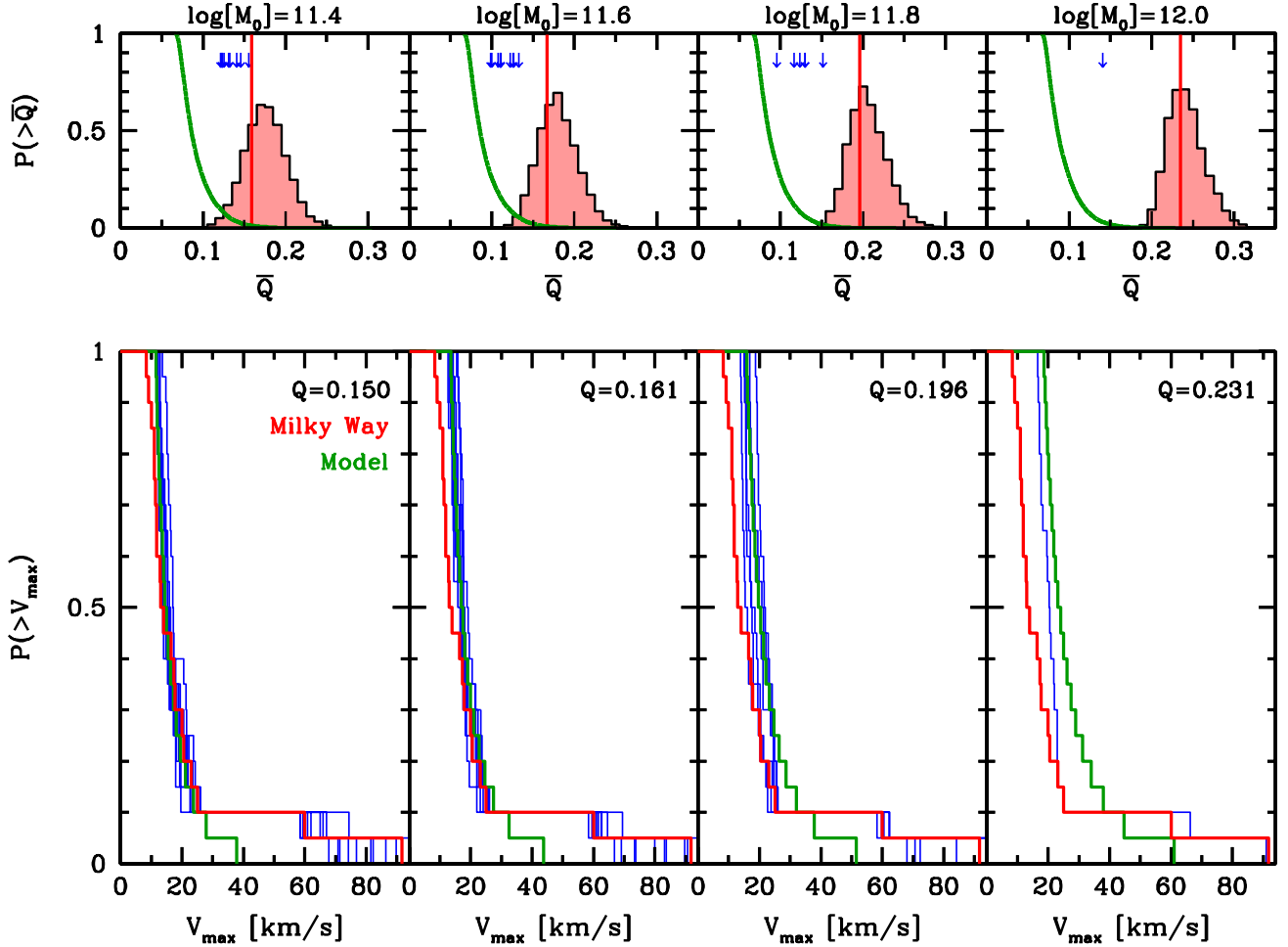


Figure 9. *Upper panels:* The thick, green curves show the cumulative probability distribution, $P(> \bar{Q})$, of the \bar{Q} statistic defined by Eqs. (13)–(14), as obtained from 10,000 model realizations for dark matter haloes in a WMAP7 cosmology. Different panels correspond to different host halo masses, as indicated. The solid, red line indicates \bar{Q}_{MW} , while the red-shaded histogram is the distribution of \bar{Q}'_{MW} from 10,000 Monte-Carlo realizations of the V_{max} -distribution of MW satellites obtained by independently drawing V_{max} values from their respective error distributions. Blue, downward pointing arrows indicate the \bar{Q} values for (some of) the model realizations that reveal a V_{max} -gap similar to the MW [i.e., $N(V_{\text{max}} > 25 \text{ km s}^{-1}) = N(V_{\text{max}} > 55 \text{ km s}^{-1}) = 2$]. *Lower panels:* Cumulative V_{max} distributions for the MW (solid, red line), the median of the 10,000 model realizations (solid, green line), and (some of) the model realizations with a V_{max} -gap similar to the MW. The Q value corresponding to the comparison of the red and green curves is indicated in the top-right corner of each panel.

$$\bar{Q}_{\text{MW}} = \frac{1}{K} \sum_{i=1}^K Q_{\text{MW},i} \quad (15)$$

Using the distribution of 10,000 \bar{Q}_i values, we can now compute $P(> \bar{Q}_{\text{MW}})$, the probability that the Λ CDM cosmology yields host haloes with \bar{Q} values as large as that of the MW. In what follows we refer to this probability as \mathcal{P}_{MW} .

Finally, we can easily adopt the Q statistic to also account for observational errors in the V_{max} values of the MW satellites. First we construct $N_{\text{MC}} = 10,000$ Monte-Carlo realization of the V_{max} -distribution of MW satellites by independently drawing V_{max} values from their respective error distributions. For simplicity, we assume that the error-distributions for V_{max} are Gaussian, with mean and standard deviation equal to the values listed in Table 1. If the V_{max} values quoted in Table 1 has separate upper and lower bounds, we assume that the standard deviation is equal to the mean of these values (i.e., we ignore any potential skew-

ness in the error distribution). Each Monte-Carlo realization results in a set S'_{MW} , where the prime is used to indicate an element of the set of N_{MC} Monte Carlo realizations. Next, for each of these S'_{MW} we compute \bar{Q}'_{MW} and the corresponding \mathcal{P}'_{MW} using the same method as described above (i.e., by comparing S'_{MW} to each of the $K = 10,000$ model realizations). The resulting distribution of \mathcal{P}'_{MW} indicates the uncertainty on \mathcal{P}_{MW} arising from the uncertainties on the individual V_{max} measurements.

We have performed the above analysis for 8 different host halo masses, $\log[M_0/(h^{-1}M_{\odot})] = 11.0, 11.2, 11.4, \dots, 12.4$, two different cosmologies (‘WMAP7’ and ‘Planck’), and 3 different values for the number of subhaloes in each set, $N = 5, 9$ and 20. Fig. 9 shows the results for the WMAP7 cosmology and $N = 20$, for four different values of M_0 , as indicated. The solid, green curve in the upper panels indicates the cumulative distribution, $P(> \bar{Q})$, obtained from the 10,000 model

realizations. This $P(> \bar{Q})$ is found to be virtually independent of host halo mass and cosmology, which is a consequence of the fact that we have normalized Q and that the *shape* of the subhalo V_{\max} function is largely invariant. The shaded histograms indicate the distributions of \bar{Q}'_{MW} , while the red, vertical line indicates \bar{Q}_{MW} . Note how \bar{Q}_{MW} shifts to larger values with increasing host halo mass, and that it is always located in the tail of the Q distribution of the model predictions, even for halo masses as low as $10^{11.4} h^{-1} M_{\odot}$.

The lower panels of Fig. 9 show the cumulative V_{\max} distribution, $P(> V_{\max})$, of the MW (red histogram), compared to the cumulative distribution of the median of the model realizations (green histogram). The latter is obtained by computing the median V_{\max} of the i^{th} ($i = 1, 2, \dots, 20$) member of all 10,000 model realizations, and roughly corresponds to the typical V_{\max} distribution of the model. The value of the Q -statistic corresponding to these two cumulative distributions is indicated in each panel, and (as expected) is similar to \bar{Q}_{MW} (indicated by the solid, vertical line in the upper panels). For a MW host halo mass of $M_0 \sim 10^{12} h^{-1} M_{\odot}$, there is a dramatic discrepancy between model and data: Not only does the model predict smaller V_{\max} for the Magellanic clouds, it also overpredicts V_{\max} for all other satellites; this is a manifestation of the TBTF problem. For a MW host halo mass of $M_0 \sim 10^{11.4} h^{-1} M_{\odot}$, on the other hand, model and data are in remarkably good agreement for the satellites with $V_{\max} < 25 \text{ km s}^{-1}$. However, the model now predicts much lower V_{\max} values for the Magellanic clouds (of the order of $30 - 40 \text{ km s}^{-1}$). There is also some tension at the low V_{\max} end ($V_{\max} \lesssim 15 \text{ km s}^{-1}$), but this reflects the onset of the ‘missing satellites’ problem, and may well reflect observational incompleteness in the inventory of MW satellites.

The thin, blue histograms show the $P(> V_{\max})$ distributions for the model realizations that reveal a V_{\max} -gap similar to the MW (i.e., $N(V_{\max} > 25 \text{ km s}^{-1}) = N(V_{\max} > 55 \text{ km s}^{-1}) = 2$). In the case of $M_0 = 10^{11.8} h^{-1} M_{\odot}$ these are the same 6 models depicted in Fig. 5, while for $M_0 = 10^{12.0} h^{-1} M_{\odot}$ only 1 (out of 10,000) model realization meets these criteria. For $M_0 = 10^{11.4} M_{\odot}$ ($10^{11.6} h^{-1} M_{\odot}$) we only show a random subset of 10 realizations, from a total of 15 (16) out of 10,000 that meet these gap-criteria. The \bar{Q} values corresponding to these model realizations are indicated as blue, downward pointing arrows in the upper panels.

In the case of $M_0 = 10^{12} h^{-1} M_{\odot}$, it is clear that TBTF is not only a problem of an unexpected V_{\max} -gap between the second and third ranked members. After all, the model that displays a gap similar to that in the MW (which in itself is extremely rare), still is an extremely poor match to the V_{\max} distribution of the other satellite galaxies (at least below $V_{\max} \sim 20 \text{ km s}^{-1}$)! In particular, the V_{\max} distribution of MW dwarf spheroidals is much broader than what is predicted by the model. Interestingly, in the case of $M_0 = 10^{11.4} h^{-1} M_{\odot}$, the models that reveal a MW-like V_{\max} -gap (which has an occurrence rate of $\sim 1.5\%$) basically are a good match to the *entire* V_{\max} distribution of dwarf spheroidals, at least down to $\sim 10 \text{ km s}^{-1}$. If it wasn't for the fact that such a low halo mass for the MW is basically ruled out by the timing argument (see e.g., Phelps, Nusser & Desjacques 2013), the space motion of Leo I (e.g., Boylan-Kolchin et al. 2013) and the kinematics of blue hor-

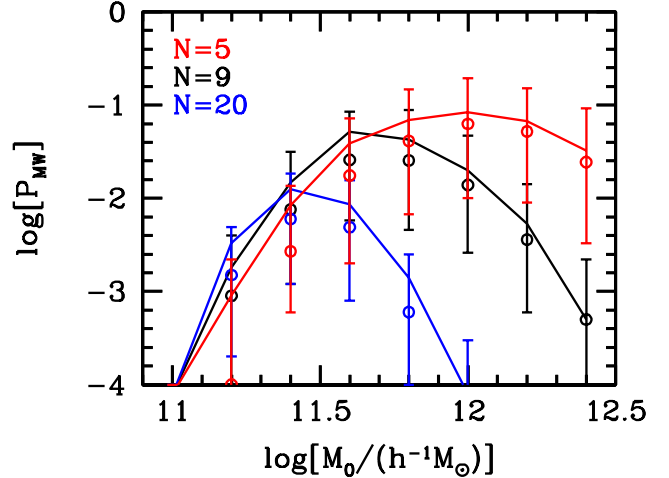


Figure 10. Solid lines show the host halo mass dependence of the probability \mathcal{P}_{MW} that the WMAP7 cosmology yields host haloes with \bar{Q} values as large as that of the MW. Open circles and error bars indicate the median and the 18 and 84 percentiles of the corresponding \mathcal{P}'_{MW} distributions, obtained from 10,000 Monte-Carlo realizations of the V_{\max} -distribution of MW satellites. Results are shown for three different values of N , as indicated.

izontal branch stars (e.g., Xue et al. 2008; Kafle et al. 2014) one might be tempted to consider this strong evidence in support of a MW halo mass of the order of $10^{11.4} h^{-1} M_{\odot}$.

Fig. 10 summarizes the results of our Q -statistic analysis. The solid lines plot the probability \mathcal{P}_{MW} as function of host halo mass for three different values of N , as indicated, while the open circles and error-bars indicate the median and the 18 and 84 percentiles of the corresponding \mathcal{P}'_{MW} distributions. These results are all based on the WMAP7 cosmology, but the results for the Planck cosmology are virtually indistinguishable. If we only focus on the five subhaloes with the largest V_{\max} values, then the inference is that the most probable mass for the MW host halo is $\sim 10^{12} h^{-1} M_{\odot}$, in good agreement with a variety of constraints (e.g., Xue et al. 2008; McMillan 2011; Boylan-Kolchin et al. 2013; Kafle et al. 2014). Furthermore, the probability that a random ΛCDM dark matter halo of that mass has a V_{\max} distribution similar to that of the MW (in terms of the Q -statistic) is $6.3^{+13}_{-5.3}\%$ (68% CL, when accounting for the errors on the individual V_{\max} measurements of the MW satellites). This does not signal concern of a potential problem for the ΛCDM paradigm.

However, when using $N = 20$ (i.e., when using the V_{\max} values of all MW satellites in Table 1 down to Willman 1, which has $V_{\max} = 8.3^{+2.7}_{-0.8} \text{ km s}^{-1}$), a very different picture emerges. In particular, the probability that a host halo of $10^{12} h^{-1} M_{\odot}$ has a V_{\max} distribution similar to that of the MW is now reduced to $< 5 \times 10^{-4}$ (at 68% CL), while the most probable MW mass has dropped to $M_0 \sim 10^{11.4} h^{-1} M_{\odot}$ (where $\mathcal{P}_{\text{MW}} = 0.6^{+1.2}_{-0.5}\%$). As is evident from the lower right-hand panel of Fig. 9, the problem is not just a large gap between ~ 25 and 55 km s^{-1} , but rather a problem regarding the *overall width* of the V_{\max} distribution of the MW satellites. Taking into account that our inventory of MW satellites may still be incomplete below $V_{\max} \sim 15 \text{ km s}^{-1}$, a more robust assessment of TBTF only uses the data of the 9 highest- V_{\max} satellite galaxies (LMC, SMC, Sagittarius,

Bootes II, Draco, Ursa Minor, Fornax, Sculptor and Leo I). In that case, we infer a MW-consistent fraction, for a host halo of $10^{12} h^{-1} M_{\odot}$, of $\mathcal{P}_{\text{MW}} = 1.4^{+3.3}_{-1.1}\%$ (68% CL). It remains to be seen how the \mathcal{P}_{MW} for $N = 20$ changes as more and better data for the population of MW dSphs continues to come available.

5 SUMMARY

In this paper we have used semi-analytical models for the substructure of dark matter haloes to assess the TBTF problem. We demonstrated that the model accurately reproduces the average subhalo mass and velocity functions, as well as their halo-to-halo variance, in high resolution N -body simulations. We then used the model to construct thousands of realizations of MW-size host haloes, which we used to investigate the TBTF problem with unprecedented statistical power.

Previous studies have formulated TBTF in different ways, which we refer to as the massive subhalo formulation, the gap formulation, and the density formulation. We have assessed TBTF in all three formulations, and compared our results to the ELVIS suite of 48 high-resolution zoom-in simulations of MW-sized host haloes (Garrison-Kimmel et al. 2014a). Overall, the results from our semi-analytical model are in excellent agreement with the ELVIS results. Using 100 mock ELVIS suites, we demonstrate, though, that the suite-to-suite variance is significant, and that a proper assessment of TBTF statistics requires simulation suites that are an order of magnitude larger than ELVIS. This motivates the use of semi-analytical models such as those presented here.

Regarding the three aforementioned formulations, our assessment of TBTF is as follows:

- **massive subhalo formulation:** according to this formulation, the MW has a deficit of massive subhaloes, defined as subhaloes with $V_{\text{max}} > 25 \text{ km s}^{-1}$ and $V_{\text{acc}} > 30 \text{ km s}^{-1}$. Whereas the MW has only two subhaloes that (most likely) meet these criteria, namely the two Magellanic clouds, most MW size host haloes have a significantly larger number of ‘massive subhaloes’, N_{MS} . We find that $\langle N_{\text{MS}} \rangle \simeq 7$ (8) and with $P(N_{\text{MS}} \leq 2) \simeq 0.1\%$ (0.05%) for a host halo mass of $M_0 = 10^{12} h^{-1} M_{\odot}$ in a WMAP7 (Planck) cosmology. However, $P(N_{\text{MS}} \leq 2)$ has a strong mass dependence, increasing to $> 10\%$ for $M_0 < 10^{11.8} h^{-1} M_{\odot}$. In addition, it also depends strongly on the exact definition of ‘massive subhaloes’. For example, changing the lower limit on V_{max} from 25 km s^{-1} to 30 km s^{-1} boosts $P(N_{\text{MS}} \leq 2)$ by an order of magnitude for $M_0 = 10^{12} h^{-1} M_{\odot}$. Finally, it is important to stress that while lowering the mass of the MW’s halo increases $P(N_{\text{MS}} \leq 2)$, it *decreases* the probability that such a halo hosts two subhaloes comparable to the Magellanic clouds.

- **gap formulation:** according to this formulation, the MW has an unexpectedly large gap in the V_{max} -rank-ordered list of its satellite galaxies. In particular, no satellite galaxies are known with a V_{max} between that of the SMC ($V_{\text{max}} = 60 \pm 5 \text{ km s}^{-1}$) and that of the Sagittarius dSph ($V_{\text{max}} = 25.1 \pm 1.5 \text{ km s}^{-1}$). If we define ‘MW-consistent’ as having two subhaloes with $V_{\text{max}} \geq 55 \text{ km s}^{-1}$ and at most one subhalo with $25 \leq V_{\text{max}} < 55 \text{ km s}^{-1}$, then we find that the MW

consistent fraction peaks at $\sim 0.6\%$ around a host halo mass of $M_0 \simeq 10^{11.8} h^{-1} M_{\odot}$. For $M_0 > 10^{12} h^{-1} M_{\odot}$ this fraction is found to be less than 0.1% , with little dependence on cosmology. As for the massive subhalo count, though, these MW consistent fractions are extremely sensitive to the exact definition of the gap; for example, changing the V_{max} -values of the gap by a mere 5 km s^{-1} can change the MW-consistent fraction by an order of magnitude.

- **density formulation:** according to this formulation, the densities of the (more massive) subhaloes are too high compared to those of the subhaloes hosting MW dSphs. In particular, PZ12 introduced a density parameter, Γ , defined by Eq. (11), and argued that whereas all MW dSphs have $0 < \Gamma < 1$, the majority of MW-size host haloes have at least one subhalo with $\Gamma \geq 1$ (such a subhalo is considered too big, or rather dense, to fail). We find that, in a WMAP7 cosmology, only $\sim 4.5\%$ (15.8%) of host haloes with $M_0 = 10^{12} h^{-1} M_{\odot}$ ($10^{11.8} h^{-1} M_{\odot}$) are MW-consistent in that $\Gamma_{\text{max}} < 1$. Note that PZ12, using a semi-analytical model similar to ours, claimed that these MW-consistent fractions are significantly higher, at 10% and 40%, respectively. As discussed in the text, we believe that their results are hampered by the use of inaccurate halo merger trees, and the oversimplified assumption that subhaloes have NFW density profiles. Finally, we emphasize that of all three TBTF formulations, the density formulation is the one most sensitive to cosmology. In particular, we find that, in a Planck cosmology, the MW-consistent fraction of host haloes with $M_0 = 10^{12} h^{-1} M_{\odot}$ is only 0.6%, rather than 4.5% in a WMAP7 cosmology.

An important, and troubling, downside with all three formulations above is that they suffer from the look-elsewhere effect and/or disregard certain aspects of the data on the MW satellite population. In an attempt to remedy these shortcomings, we have devised a new statistic which is ‘blind’, in that it doesn’t require the pre-selection of some particular scale (i.e., a particular V_{max} , V_{acc} and/or Γ value), treats all data on equal footing, and also allows for a straightforward treatment of errors in the V_{max} measurements of individual MW satellites. Similar in spirit to the Kolmogorov-Smirnov (KS) test, this Q -statistic, defined by Eq. (13), compares two cumulative distributions. It provides a (conveniently normalized) measure for the absolute value of the area between two cumulative distributions, and has the advantage over the KS-test that it has equal sensitivity throughout the distributions. As a consequence, it is equally sensitive to the offset between two distributions as to a difference in the spread.

Using this Q -statistic to compare the V_{max} distribution of the 9 MW satellites with the largest V_{max} measurements to that of dark matter subhaloes in our model realizations, we infer a MW-consistent fraction, for a host halo of $10^{12} h^{-1} M_{\odot}$, of $\mathcal{P}_{\text{MW}} = 1.4^{+3.3}_{-1.1}\%$, where the upper and lower bound reflect uncertainties due to the errors on the individual V_{max} errors. This is similar to the MW-consistent fraction inferred in the density formulation, but significantly larger than what is inferred from the gap-statistic. However, the latter is severely hampered by the look-elsewhere effect, and does not reflect a proper assessment of the TBTF severity.

To conclude, it is difficult to express the severity of

TBTF in a single number. In general, TBTF is (slightly) more problematic in a Planck cosmology, compared to a WMAP7 cosmology, and is minimized if the virial mass of the MW's host halo falls in the range $3 - 6 \times 10^{11} h^{-1} M_{\odot}$. Such a low MW mass, however, is basically ruled out by a variety of independent constraints (e.g., Xue et al. 2008; McMillan et al. 2011; Boylan-Kolchin et al. 2013; Phelps et al. 2013; Kafle et al. 2014). Assuming instead a host halo mass of $10^{12} h^{-1} M_{\odot}$, and using only data on the 9 known satellite galaxies with $V_{\max} > 15 \text{ km s}^{-1}$, both the density formulation and the Q -statistic suggest a MW-consistent fraction of the order of a few percent, something which we do not consider particularly challenging for the Λ CDM paradigm. However, if it turns out that the inventory of MW satellite galaxies is complete to $\sim 8 \text{ km s}^{-1}$ (i.e., future surveys uncover no new MW satellite galaxies with $V_{\max} \gtrsim 8 \text{ km s}^{-1}$), then it is clear that the spread in V_{\max} values for the 20 highest V_{\max} -ranked satellites is utterly inconsistent with Λ CDM predictions. In that case, we either (i) have systematically underestimated the V_{\max} values (by about a factor of two) of all MW dwarf spheroidals, (ii) the process of galaxy formation significantly lowers the central densities (and hence V_{\max}) of the subhaloes hosting dwarf spheroidals, or (iii) the Λ CDM paradigm is actually falsified. In this respect, it remains to be seen whether baryonic effects, such as those discussed in Zolotov et al. (2012), Brooks & Zolotov (2014), and Arraki et al. (2014), can give rise to satellite populations in hydro-dynamical simulations with V_{\max} distributions in better agreement with observations. We hope that the Q -statistic introduced here will prove useful to compare such simulations to the data.

ACKNOWLEDGMENTS

We are grateful to the people responsible for the Bolshoi and ELVIS simulations for making their halo catalogs publicly available, the anonymous referee for an insightful report that helped to improve the presentation, and to the following individuals for their advice and useful discussions: Peter Behroozi, Mike Boylan-Kolchin, Shea Garrison-Kimmel, Andrew Hearin, and Duncan Campbell.

REFERENCES

- Anderhalden D., Schneider A., Maccio A. V., Diemand J., Bertone G., 2013, JCAP, 3, 14
- Arraki K. S., Klypin A., More S., Trujillo-Gomez S., 2014, MNRAS, 438, 1466
- Behroozi P. S., Wechsler R. H., Wu H.-Y., 2013a, ApJ, 762, 109
- Behroozi P. S., Wechsler R. H., Wu H.-Y., Busha M. T., Klypin A. A., Primack J.R., 2013b, ApJ, 763, 18
- Benson A. J., Frenk C. S., Lacey C. G., Baugh C. M., Cole S., 2002, MNRAS, 333, 177
- Boylan-Kolchin M., Springel V., White S. D. M., Jenkins A., Lemson G., 2009, MNRAS, 398, 1150
- Boylan-Kolchin M., Bullock J. S., Kaplinghat M., 2011, MNRAS, 415, L40
- Boylan-Kolchin M., Bullock J. S., Kaplinghat M., 2012, MNRAS, 422, 1203
- Boylan-Kolchin M., Bullock J. S., Sohn S. T., Besla G., van der Marel R. P., 2013, ApJ, 768, 140
- Brooks A. M., Zolotov A., 2014, ApJ, 786, 87
- Bryan G. L., Norman M. L., 1998, ApJ, 495, 80
- Busha M. T., Marshall P. J., Wechsler R. H., Klypin A., Primack J., 2011, ApJ, 743, 40
- Cautun M., Hellwing W. A., van de Weygaert R., Frenk C. S., Jones B. J. T., Sawala T., 2014a, MNRAS, 445, 1820
- Cautun M., Frenk C. S., van de Weygaert R., Hellwing W. A., Jones B. J. T., 2014b, MNRAS, 445, 2049
- de Blok W. J. G., 2010, Advances in Astronomy, 2010, 789293
- DES Collaboration et al. , 2015, preprint (arXiv:1503.02584)
- Diemand J., Kuhlen M., Madau P., Zemp M., Moore B., Potter D., Stadel J., 2008, Nature, 454, 735
- di Cintio A., Knebe A., Libeskind N. I., Yepes G., Gottlober S., Hoffman Y., 2011, MNRAS, 417, L74
- Dutton A. A., Courteau S., de Jong R., Carignan C., 2005, ApJ, 619, 218
- Einasto J., 1965, Trudy Ast. Int. Alma-Ata, 5, 87
- Flores R. A., Primack J. R., 1994, ApJ, 427, L1
- Gan J., Kang X., van den Bosch F. C., Hou J., 2010, MNRAS, 408, 2201
- Garrison-Kimmel S., Boylan-Kolchin M., Bullock J. S., Lee K., 2014, MNRAS, 438, 2578
- Garrison-Kimmel S., Boylan-Kolchin M., Bullock J. S., Kirby E. N., 2014, MNRAS, 444, 222
- Giocoli C., Tormen G., van den Bosch F. C., 2008, MNRAS, 386, 2135
- Giocoli C., Tormen G., Sheth R. K., 2012, MNRAS, 422, 185
- Gross E., Vitells O., 2010, The European Phys. J., 70, 525
- Hayashi E., Navarro J. F., Taylor J. E., Stadel J., Quinn T., 2003, ApJ, 584, 541
- Jiang F., van den Bosch F. C., 2014a, MNRAS, 440, 193
- Jiang F., van den Bosch F. C., 2014b, preprint (arXiv:1403.6827)
- Kafle P. R., Sharma S., Lewis G. F., Bland-Hawthorn J., 2014, ApJ, 794, 59
- Kallivayalil N., van der Marel R. P., Besla G., Anderson J., Alcock C., 2013, ApJ, 764, 161
- Klypin A., Kravtsov A. V., Valenzuela O., Prada F., 1999, ApJ, 522, 82
- Klypin A., Trujillo-Gomez S., Primack J., 2011, ApJ, 740, 102
- Kravtsov A. V., Klypin A. A., Khokhlov A. M., 1997, ApJS, 111, 73
- Kuhlen M., 2010, Advances in Astronomy, 162083
- Kuhlen M., Madau P., Krumholz M. R., 2013, ApJ, 776, 34
- Kuzio de Naray R., McGaugh S. S., de Blok W. J. G., 2008, ApJ, 676, 920
- Larson D., et al. , 2011, ApJS, 192, 16
- Lovell M. R., et al. , 2012, MNRAS, 420, 2318
- Ludlow A. D., et al. , 2013, MNRAS, 432, 1103
- Maccio A. V., Fontanot F., 2010, MNRAS, 404, L16
- Madau P., Diemand J., Kuhlen M., 2008, ApJ, 679, 1260
- Mao Y.-Y., Williamson M., Wechsler R. H., 2015, preprint (arXiv:1503.02637)
- Martinez G. D., 2013, preprint (arXiv:1309.2641)
- McConnachie A. W., 2012, AJ, 144, 4
- McMillan P.J., 2011, MNRAS, 414, 2446
- Moore B., 1994, Nature, 370, 629
- Moore B., Quinn T., Governato F., Stadel J., Lake G., 1999, MNRAS, 310, 1147
- Navarro J. F., Frenk C. S., White S. D. M., 1997, ApJ, 490, 493
- Oguri, M., Lee, J., 2004, MNRAS, 355, 120
- Oh S.-H., Brook C., Governato F., Brinks E., Mayer L., de Blok W. J. G., Brooks A., Walter F., 2011, AJ, 142, 24
- Parkinson H., Cole S., Helly J., 2008, MNRAS, 383, 557
- Peñarrubia J., Benson A. J., 2005, MNRAS, 364, 977
- Peñarrubia J., Navarro J. F., McConnachie A. W., 2008, ApJ, 673, 226
- Peñarrubia J., Benson A. J., Walker M. G., Gilmore G., McConnachie A. W., Mayer L., 2010, MNRAS, 406, 1290
- Phelps S., Nusser A., Desjacques V., 2013, ApJ, 775, 102

- Planck Collaboration et al. , 2014, *A&A*, 571, 16
- Polisensky E., Ricotti M., 2014, *MNRAS*, 437, 2922
- Purcell C. W., Zentner A. R., 2012, *JCAP*, 12, 7
- Rashkov V., Madau P., Kuhlen M., Diemand J., 2012, *ApJ*, 745, 142
- Reed D., Governato F., Quinn T., Gardner J., Stadel J., Lake G., 2005, *MNRAS*, 359, 1537
- Rocha M., Peter A. H. G., Bullock J. S., Kaplinghat M., Garrison-Kimmel S., Onorbe J., Moustakas L. A., 2013, *MNRAS*, 430, 81
- Rodriguez-Puebla A., Avila-Reese V., Drory N., 2013, *ApJ*, 767, 92
- Rodriguez-Puebla A., Avila-Reese V., Drory N., 2013, *ApJ*, 773, 172
- Shao S., Gao L., Theuns T., Frenk C. S., 2013, *MNRAS*, 430, 2346
- Somerville R. S., Kolatt T. S., 1999, *MNRAS*, 305, 1
- Springel V., White M., Hernquist L., 2001, *MNRAS*, 549, 681
- Springel V., et al. , 2008, *MNRAS*, 391, 1685
- Strigari L. E., Bullock J. S., Kaplinghat M., Diemand J., Kuhlen M., Madau P., 2007, *ApJ*, 669, 676
- Taffoni G., Mayer L., Colpi M., Governato F., 2003, *MNRAS*, 341, 434
- Taylor J. E., Babul A., 2001, *ApJ*, 559, 716
- Taylor J. E., Babul A., 2004, *MNRAS*, 348, 811
- Taylor J. E., Babul A., 2005a, *MNRAS*, 364, 515
- Taylor J. E., Babul A., 2005b, *MNRAS*, 364, 535
- Tollerud E. J., Bullock J. S., Strigari L. E., Willman B., 2008, *ApJ*, 688, 277
- Tollerud E. J., Boylan-Kolchin M., Bullock J. S., 2014, *MNRAS*, 440, 3511
- Trachternach C., de Blok W. J. G., Walter F., Brinks E., Kennicutt R. C. Jr., 2008, *AJ*, 136, 2720
- van den Bosch F. C., Swaters R. A., 2001, *MNRAS*, 325, 1017
- van den Bosch F. C., 2002, *MNRAS*, 331, 98
- van den Bosch F. C., Tormen G., Giocoli C., 2005, *MNRAS*, 359, 1029 (vdB05)
- van den Bosch F. C., Jiang F., 2014, preprint (arXiv:1403.6835)
- van den Bosch F. C., Jiang F., Hearin A., Campbell D., Watson D., Padmanabhan N., 2014, *MNRAS*, 445, 1713
- van der Marel R. P., Kallivayalil N., 2014, *ApJ*, 781, 121
- Vera-Ciro C. A., Helmi A., Starkenburg E., Breddels M. A., 2013, *MNRAS*, 428, 1696
- Vogelsberger M., Zavala J., Loeb A., 2012, *MNRAS*, 423, 3740
- Wang J., Frenk C. S., Navarro J. F., Gao L., Sawala T., 2012, *MNRAS*, 424, 2715
- Wechsler R. H., Bullock J. S., Primack J. R., Kravtsov A. V., Dekel A., 2002, *ApJ*, 568, 52
- Wolf J., Martinez G. D., Bullock J. S., Kaplinghat M., Geha M., Munoz R. R., Simon J. D., Avedo F. F., 2010, *MNRAS*, 406, 1220
- Wu H.-Y., Hahn O., Wechsler R. H., Behroozi P. S., Mao Y.-Y., 2013, *ApJ*, 767, 23
- Xue X. X., et al. , 2008, *ApJ*, 684, 1143
- Yang X., Mo H. J., Zhang Y., van den Bosch F. C., 2011, *ApJ*, 741, 13
- Zentner A. R., Bullock J. S., 2003, *ApJ*, 598, 49
- Zentner A. R., Berlind A. A., Bullock J. S., Kravtsov A. V., Wechsler R. H., 2005, *ApJ*, 624, 505
- Zhao D. H., Jing Y. P., Mo H. J., Borner G., 2009, *ApJ*, 707, 354
- Zhang J., Fakhouri O., Ma C.-P., 2008, *MNRAS*, 389, 1521
- Zolotov A., et al. , 2012, *ApJ*, 761, 71